DESIGN AND FABRICATION OF A VARIABLE STIFFNESS LINK FOR USE IN A MORPHABLE UNMANNED AIR VEHICLE

by

Brad M. Boyerinas

Bachelor of Science in Mechanical Engineering, University of Pittsburgh, 2006

Submitted to the Graduate Faculty of

the Swanson School of Engineering in partial fulfillment

of the requirements for the degree of

Master of Science

University of Pittsburgh

2009

UNIVERSITY OF PITTSBURGH

SWANSON SCHOOL OF ENGINEERING

This thesis was presented

by

Brad M. Boyerinas

It was defended on

December 12, 2008

and approved by

William W. Clark, Professor, Department of Mechanical Engineering and Materials Science

William S. Slaughter, Associate Professor, Department of Mechanical Engineering and Materials Science

Thesis Advisor: Lisa Mauck Weiland, Assistant Professor, Department of Mechanical Engineering and Materials Science

DESIGN AND FABRICATION OF VARIABLE STIFFNESS LINK FOR USE IN MORPHABLE UNMANNED AIR VEHICLE

Brad M. Boyerinas, M.S.

University of Pittsburgh, 2009

Morphing structures have recently been researched by scientists and engineers due to their ability to adapt to a physical environment and increase the odds of performance and survival. One area of implementation, aeronautics, has been of specific interest since aircraft are commonly called upon to perform in several varying scenarios, some of which the aircraft is ill-suited for survival. These varying scenarios are most commonly experienced by military aircraft where the capabilities of efficient cruising, straight-line speed, and agile maneuvering can be encountered in just one flight.

This thesis focuses on the development of a smart structural link that has the capability of being deformed and locked in several positions. The link was designed for and tested in a morphable unmanned air vehicle where the wings can both sweep and morph for greater aerodynamic performance under different conditions. This structural link bends to high degrees of deformation while its main constituent, shape memory polymer, is thermally activated and possesses a very low stiffness. The link setup was tested in the Kirsten Wind Tunnel at the University of Washington and was successfully implemented for several cycles.

TABLE OF CONTENTS

LIST OF TABLES

LIST OF FIGURES

ACKNOWLEDGEMENTS

First, I would like to thank my advisors Dr. Lisa Weiland and Dr. William Clark. I am grateful for having the opportunity to work in the Vibration and Control Lab as an undergraduate student as well as a graduate student. I would also like to thank other members, past and present, of the Vibration and Control Lab for their insight. Last and not least, I would like to thank my family for their support and encouragement throughout my academic career.

1.0 INTRODUCTION

Traditional engineering materials often present limitations when designing structural elements for large deflections. In fact, the equation of the elastic curve, formulated by Jacob Bernoulli in 1694 and still being used in practice today, was simplified to exclude geometric nonlinearity since most structural materials can bear only small deflections. However, modern research has produced a class of materials, called smart materials, that can significantly change mechanical properties when an external stimulus is applied to the surrounding environment. Two such materials, shape memory polymers and alloys, can become significantly less stiff when a stimulus is applied, as well as display the shape memory effect. These activation stimuli include thermal or light energy for shape memory polymers and thermal energy or mechanical loading for shape memory alloys. This behavior allows high deformation properties and can also enable active control of deformation when a load is applied to the structure.

Interest has recently risen in using smart materials for morphing and deployable structures (CRG Inc. 2008). More specifically, morphing has grabbed the attention of aerospace engineers. For aerospace designers to continue to make aircraft more versatile, the cross section of the wing geometry as well as the angle of the wing with the fuselage must be controllable. Instead of creating linkages with conventional materials that are considered inextensible and rigid, this thesis will propose a novel approach to the problem: implement a structural member that deforms in order to facilitate wing shape change. This linkage, dubbed the Smart Link, will

be designed to stand up to the rigors of aerodynamic load in an unmanned air vehicle and also be able to soften upon stimulus, morph to a desired position, and harden again with the stimulus removed. Shape memory polymer is employed because of its large change in modulus at the transition temperature.

Veriflex, a commercially available shape memory polymer (SMP) available from CRG Inc., is employed for its thermally induced variable modulus properties and is coupled with nitinol super-elastic alloy. The nitinol serves as the back bone of the linkage and prevents out of plane shear displacement when the SMP is thermally activated as well as providing elasticity to return the link to its normal position. The nitinol was also chosen due to its super-elastic properties so that yielding would not occur during bending. The Smart Link is displayed in Figure 1.1.

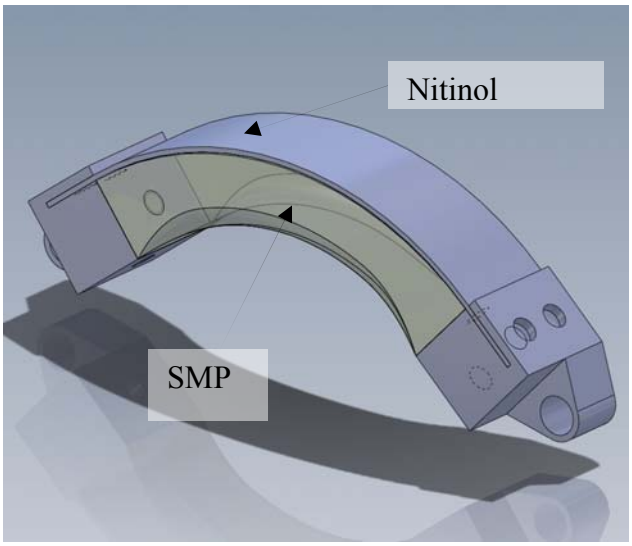

Figure 1.1. 3d rendering of Smart Link

This thesis will display the evolution of the smart link through material selection, design, testing and experimental setup, and theoretical analysis.

1.1 OUTLINE

A literature review is presented in subsequent pages, briefly describing the behavior of shape memory polymers and alloys as well as how such materials can be successfully utilized in a morphing aircraft structure. Next, the motivation for using a smart material concept in place of a traditional mechanical device is explained. Then, design specifications for the Smart Link are described and the design steps are laid out. Theoretical analysis of the mechanical and thermal behavior of the link is shown next. Test results from wind tunnel testing and the link performance are listed. Lastly, future work and suggested improvements close the thesis.

2.0 LITERATURE REVIEW

Significant research involving smart materials has been conducted with applications including medical uses, vibration control, energy harvesting, and morphing structures. The following review will focus on the properties of shape memory polymers and superelastic shape memory alloys as well as prior work involving morphing aircraft and other variable modulus morphing concepts, as these topics are most pertinent to the research at hand.

2.1 SHAPE MEMORY POLYMER

Shape memory materials are unique in that they can be deformed into a seemingly plastic state but have the ability to 'remember' or spring back into their initial configuration after a stimulus is applied. When a shape memory polymer is cast, its shape is known as the initial configuration. This configuration will be maintained when the environment is below that activation or the glass transition temperature. The polymer will then become very soft when heated above glass transition, generally possessing a Young's modulus many orders of magnitude lower than when below the transition temperature, as displayed in Figure 2.1. Then, if the sample is held in this new configuration as the sample cools, the polymer will continue to hold this newly configured shape without any external load applied. The next time it is heated above the glass transition

temperature, the polymer will spring back to its initial configuration if not physically constrained.

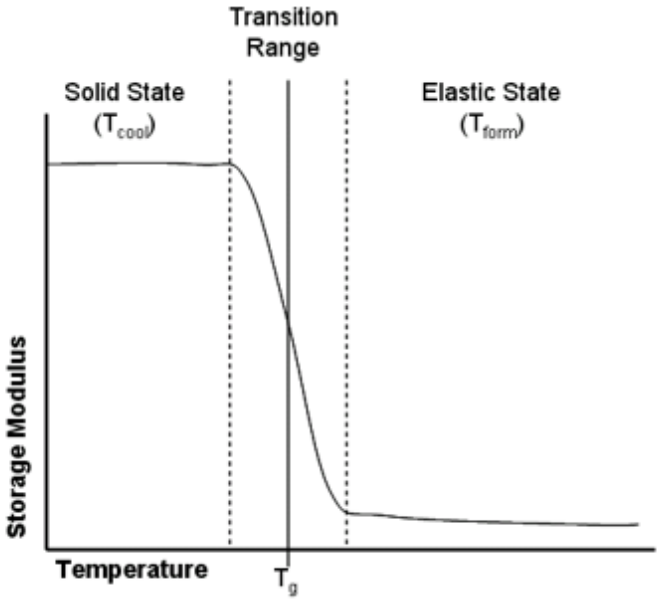

Figure 2.1. Thermo-elastic response of Veriflex SMP (CRG Industries LLC., 2008)

This memory behavior has created interest within the scientific community since it will allow researchers to create novel actuators and morphing systems, as is the basis of this thesis. Figure 2.2 demonstrates the complete memory cycle of SMP.

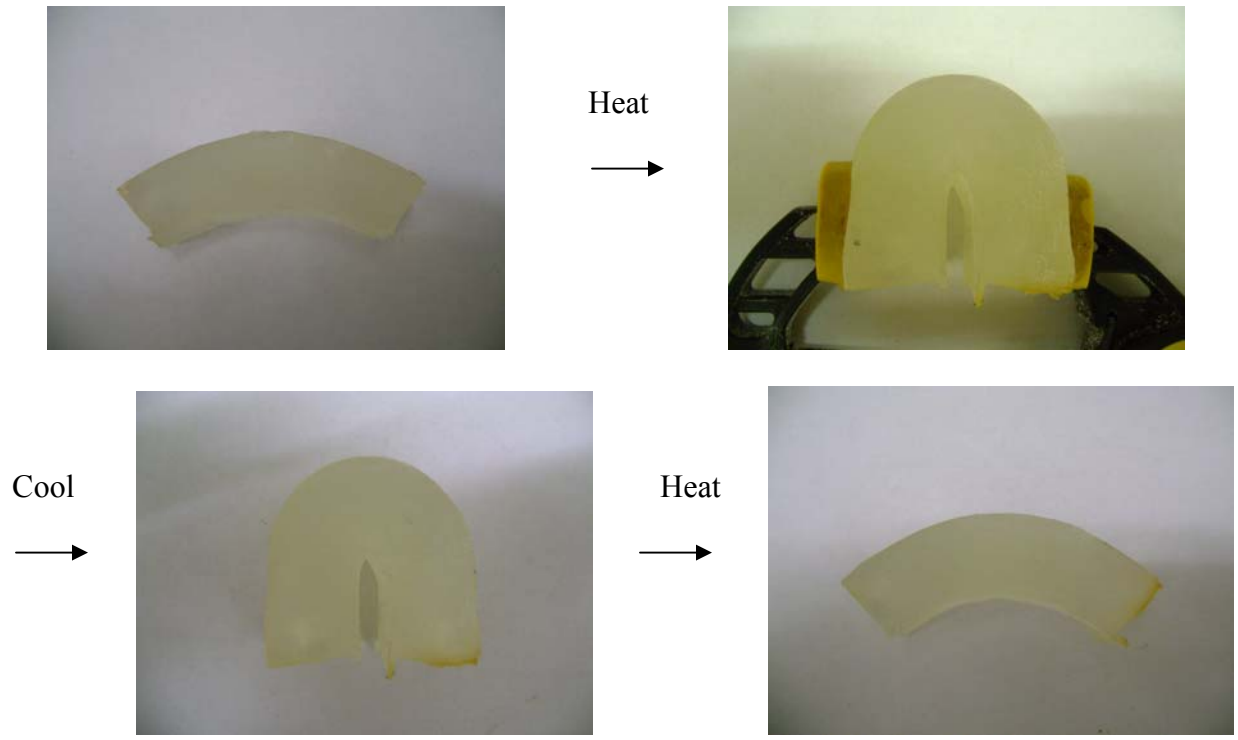

Figure 2.2. One complete thermal cycle of Veriflex shape memory polymer

Extensive review papers by Sandstrom and Miyazaki in 1998 and Liu, Qin, and Mather in 2007 exhaustively describe shape memory polymers in terms of mechanisms, history, and applications.

L.B. Vernon was one of the first to document shape memory effect in polymers while claiming a United States patent in 1941. His work produced a methacrylic acid ester that would return to its initial state after exposure to a thermal stimulus. The feasibility of SMP as a useful engineering material was realized in 1967 when covalently cross-linked polyethylene was used in tubing and films that could shrink after being exposed to a thermal stimulus (Sandstrom et al., 1998).

Compared to other smart materials, SMPs possess several distinct advantages. First, they can withstand higher degrees of elastic deformation, with recoverable strain up to 200% in most cases (some cases approach 800%). They can also have a tailored activation temperature making

implementation into a specific application straightforward. SMP can also be synthesized as a biodegradable polymer, proving several uses in the medical field including active sutures (Sandstrom et al., 1998).

Shape memory polymers have gained the interest of the medical community not only since they can be biocompatible, but also since they can be implemented in scenarios where non-invasive surgical methods are required. The shape memory effect can be utilized in this case so that a coil of the polymer is inserted through a wound or incision and then heated to contract and tightly close the opening. This process of suturing is useful because a surgeon is not required to pull long lengths of material through a wound which can be difficult and hazardous in tight areas.

Even if the entire suture is not comprised of shape memory polymer, partial use in the knot section may make surgical operations much easier. As shown in Figure 2.3, a loosely tied knot in a fiber of SMP is capable of tightening itself in a short amount of time (20 seconds) when exposed to an environment over its transition temperature (40 degrees C). Both ends of the fiber were fixed in order for the knot to tighten.

Figure 2.3. Loosely tied knot in SMP fiber tightened in 20 seconds at 40 °C (Smart suture, 2002)

Similar to the Smart Link concept, McKnight and Henry (2005) at HRL Laboratories created a model involving morphing structure capability that utilizes the variable modulus capabilities of SMP. The polymer used in their setup is Diaplex 5510 and is capable of dropping to a storage modulus of ~50 Mpa from ~2Gpa during thermal activation. The proposed setup involves a composite structure of rigid rectangular elements embedded within a shape memory polymer matrix, as seen below in Figure 2.4.

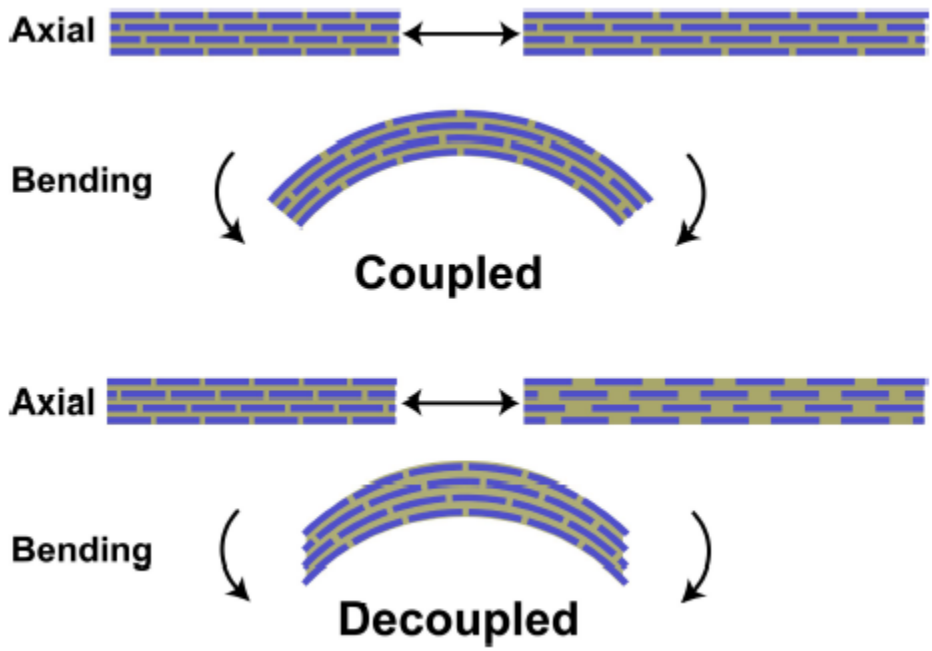

Figure 2.4. Deformation modes for variable stiffness composite structure (McKnight et al., 2005)

When the SMP is under the glass transition temperature, the rigid links and polymer matrix are coupled, creating a structure that will deform in a continuous manner if both link and polymer elastic moduli are similar. When the SMP is thermally activated, the structure will become decoupled with the polymer region becoming more compliant. This contrast in stiffness allows the structure to elongate or bend with significantly less effort than when the polymer is not activated. However, in composite cases similar to the one shown above, the polymer must tolerate a shear strain of up to 100% in order for the composite structure to deform to only 5%.

If the structure needs to be very stiff in the hard state, a smaller volume of SMP will be required, forcing the polymer to undergo even larger strains. This factor exemplifies the possible limitations of smart material composites, since a large strength to displacement ratio may cause the polymer matrix to fail (McKnight et al., 2005).

SMP has also previously been used in morphing wing research. In 2008, Rauscher developed a morphable tile comprised of SMP inside of a rigid frame, as shown below. Nichrome wires were placed within the polymer region to heat and activate the SMP. In concept, an entire lattice of these tiles would cover the surface of the wing and permit shear displacement when the shape memory polymer was softened. This lattice would allow both a rotation of the wing and a change in surface area. In practice this design worked in that it was rigid and allowed shearing when activated as well as a flat, unbuckled inner surface during modest shear deflection. However, during large shear deformations, the SMP region would buckle, as shown in Figure 2.5. A very large force was required to induce the proper shear displacement.

Figure 2.5. SMP tile after shear displacement (Rauscher 2008)

2.2 SHAPE MEMORY ALLOYS

Shape memory alloys can be more attractive to engineers since they are generally more robust than SMP in terms of strength and durability due to a higher Young's modulus. When comparing shape memory alloys to conventional materials there are two distinct differences in mechanical behavior: the shape memory and superelastic effects. Shape memory is achieved by recovering very large mechanical strains when the alloy is exposed to an environment above the transition temperature. The superelastic effect occurs when the metal is exposed to very large strain during loading and then recovers entirely during unloading, as shown in Figure 2.6. Simply put, nitinol is a metal that can bend to an extreme unlike other common engineering materials and return to its original state without plastic deformation. Since the smart link design utilizes only the superelastic effect, a further explanation of shape memory performance will be omitted.

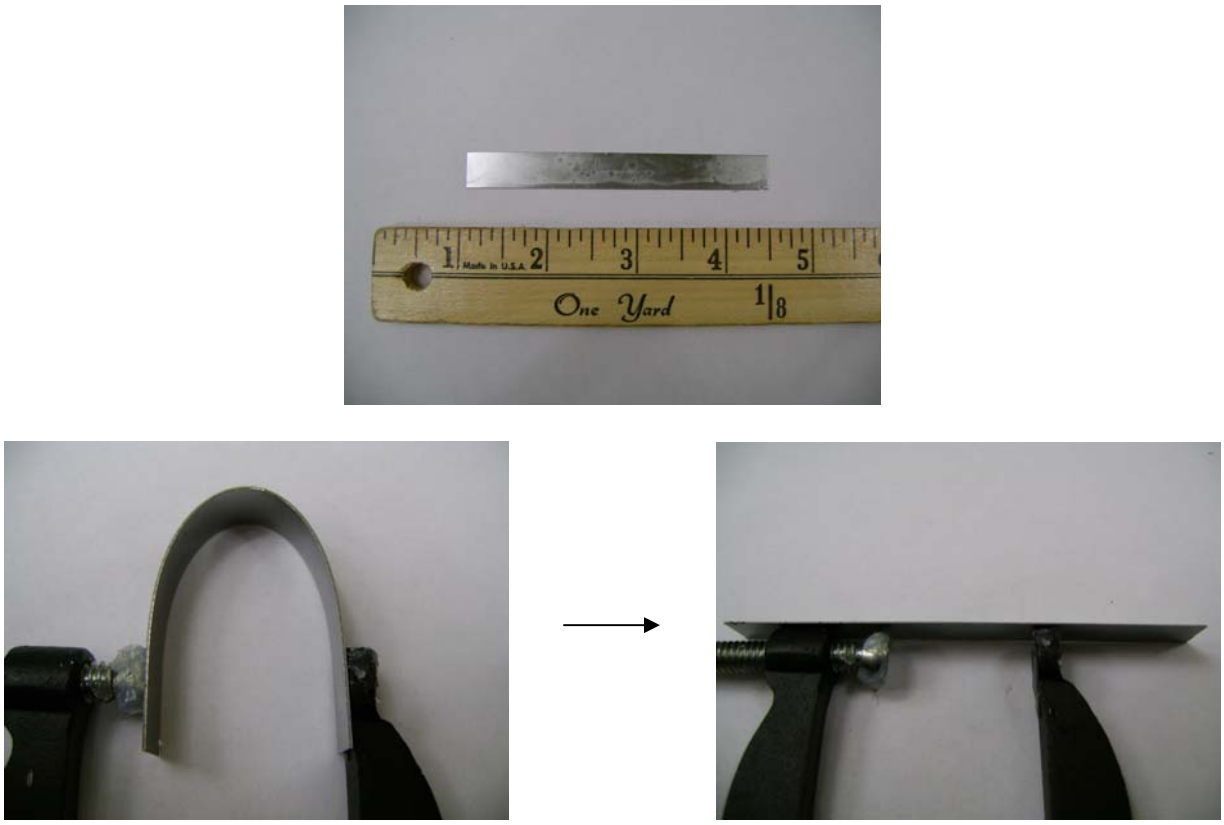

Figure 2.6. Nitinol beam under deformation then unloaded to initial configuration

Nitinol, a nickel-titanium alloy and the SMA used in the smart link, can recover very large strains in a superelastic manner due to phase transformation. This phase transformation can be due to either applied thermal energy (shape memory) or applied loading (superelasticity). In a stress-free state above the austenitic transformation temperature, nitinol will exist in the austenite phase. As a load is applied, the metal will display a linear elastic response until the critical stress, σ_{cr}, is reached, as seen in region A on Figure 2.7. At this point in loading, the phase transformation will begin in the affected volume with the structure changing to a martensite phase, noted in region B. Continued straining displays an apparent plastic response. This martensitic phase makes the alloy much softer and allows large strain with very little added stress. Then, as the structure is unloaded, a linear elastic response is observed, as seen in region C. As the response approaches region D, the phase abruptly starts a transition back into

austenite, and exhibits a reversible plastic response. As the unloading approaches the initial state, the curve again resembles a linear return to the unloaded state. The overall cycle represents a hysteresis curve, with the area enclosed displaying the work done on the body (Leo, 2007).

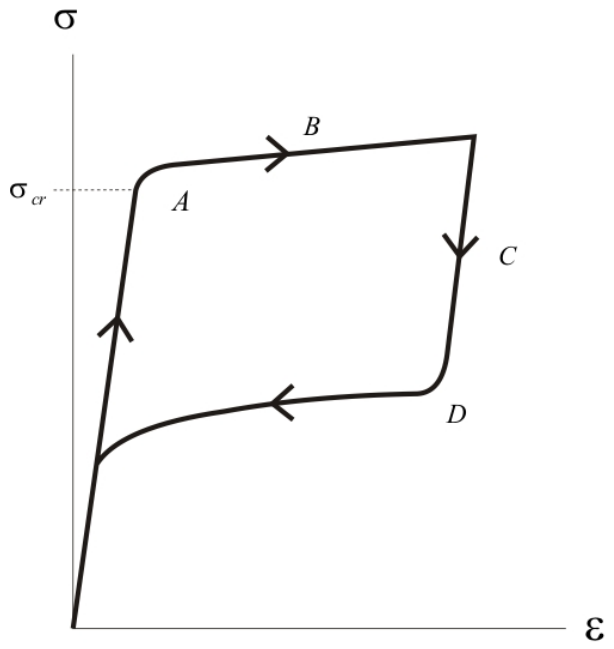

Figure 2.7. Mechanical response of superelastic nitinol

2.3 BACKGROUND OF MORPHING AIRCRAFT

Until the success of the Wright brothers first flight, mankind tried and failed to mimic the flying action of birds. Several early designs dating back to Leonardo da Vinci and the renaissance involved foldable, flapping wings to attempt flight initiation and control (U.S. Air Force, 2008). With the advent of powerful rotary and jet engines, airplane structures took on a static design, requiring the wings to only make lift and not thrust. This current design philosophy requires

engineers to find a medium between dynamic performance and maneuverability versus drag and efficiency. Even with superior design, physical limitations prevent an aircraft from being able to be both extremely agile and efficient. This dilemma affects military aircraft the greatest since they are often called upon to cruise very long distances and then engage or evade enemies in a responsive manner. A designer must decide which scenarios the airplane will encounter most and then adjust characteristics so that the plane will perform admirably in its preferred regime.

If an aircraft can morph in flight to significantly change its aerodynamic properties, then one design will be able to satisfy several performance criteria. This will prevent the need for an entire fleet of specialized aircraft and improve the chances of success if an aircraft faces unexpected circumstances that it was not intended to encounter. As exemplified with the F-18 aeroelastic wing concept mentioned below, novel morphing technologies may lighten the gross weight of the aircraft as well as improving dynamic performance.

Jha and Kudva (2004) outlined seven technical challenges that designers must address when designing a morphing aircraft. The first is creating optimal design configurations for each state. The designer must identify an optimal configuration for each scenario that the aircraft will encounter (loiter, dash, etc.). Next, the structural integrity of the morphing wings must be considered since the skin must be very soft and pliable to allow drastic shape change. In turn, the overall rigidity of the wing will be compromised to a certain degree. Third, actuation forces must be minimized to decrease weight and power consumption within the aircraft and this aspect may hinder wing strength since softer materials will be required. Fourth, the skin design must maintain a smooth profile and hold required airfoil shapes at each configuration. Next, the control of the wings has to be implemented so that the system is reliable in very high frequency operation and also so that minimal human input is required when changing wing shape for

various conditions. Also, the engine of the plane must be equipped to handle all possible scenarios that may be encountered, requiring acceptable performance at all speeds. Finally, the integration of all of the subsystems listed above must be placed into a compact space and not hinder the motion of the wing. New materials and technologies must be developed in order for the morphing system to require a moderate amount of power for operation and be light enough to have appreciable flight characteristics.

When considering the preceding challenges, material development and integration will be the most difficult. A suitable candidate for an active morphing material must possess a high degree of change when stimulated. Also, employing the infrastructure to activate the morphing process must not impede deformation by any appreciable amount. In other words, heating pads or electrodes for thermal or electrically stimulated material may prevent high levels of deformation since these items themselves may be very stiff. Scientists must discover a method to activate the morphing section of a wing without prohibiting movement for practical implementation. The successful test of the Smart Link shows that implementing conventional stimulation techniques such as heating pads may hold promise with morphing design.

2.4 MODERN MORPHING AIRCRAFT DEVELOPMENTS

Aerospace technology has advanced to a point where static wing design has reached its pinnacle and wings must be able to physically adapt for optimal performance in a given scenario. Prior adaptive wing design includes the use of a pin joint to rotate the wing on an axis, as seen in the F-14 Tomcat pictured in Figure 2.8, so that the wing can sweep close to the fuselage to decrease drag.

Figure 2.8. F-14 Tomcat in flight (Grumman Aerospace Corporation, 2008)

More recently, the NASA Dryden Flight Research Center successfully completed a test flight of the Active Aeroelastic Wing (AAW) F-18 combat fighter in 2002 (NASA, 2008). This aircraft, seen in Figure 2.9 during testing, is capable of modifying the twist of the wings to provide greater control capabilities while performing roll maneuvers. This wing warping technology proved so effective that the prototype was able to roll approximately fifteen to twenty percent of what a production F-18 is capable of without the use of conventional flight control devices. Researchers at Dryden claim that aeroelastic wing technology can lower gross weight by seven to ten percent in a transonic plane and up to eighteen percent on a supersonic plane, adding to overall flight efficiency.

Figure 2.9. Morphing F-18 fighter wing in torsion (AIAA, 2008)

In the last several years, government funding spearheaded by DARPA has pushed morphing research into academia and private industry (Jha et al., 2004). NextGen Aeronautics, an advanced aeronautics design company based in Torrance, CA, has developed and tested two morphing unmanned air vehicles (UAVs). One of these aircraft, the MFX-1, is a 100 pound jet powered and remotely controlled and also has morphing wing capabilities.

In August 2006, the MFX-1 underwent a successful flight test where the sweeping wing design underwent a surface area change of approximately 40% with an electric motor as the primary actuator. NextGen stated the main purposes of the flight tests as: demonstrating capability of successful operation and flight stability and control, and developing piloting procedures that will be necessary for testing of future morphing UAVs (NextGen, 2008).

The first aerial test was unsuccessful due to geometric asymmetry between the wings. This caused the aircraft to roll uncontrollably to one side and stall. After addressing this problem, the MFX-1 flew effectively on August 1, 2006 at altitudes ranging between 400-600 feet and airspeeds ranging between 100-120 knots. In less than 15 seconds, the wing span

changed 30% and the wing sweep varied from 15 to 35 degrees. Change in wing orientation can be seen in the Figure 2.10 below (NextGen, 2008).

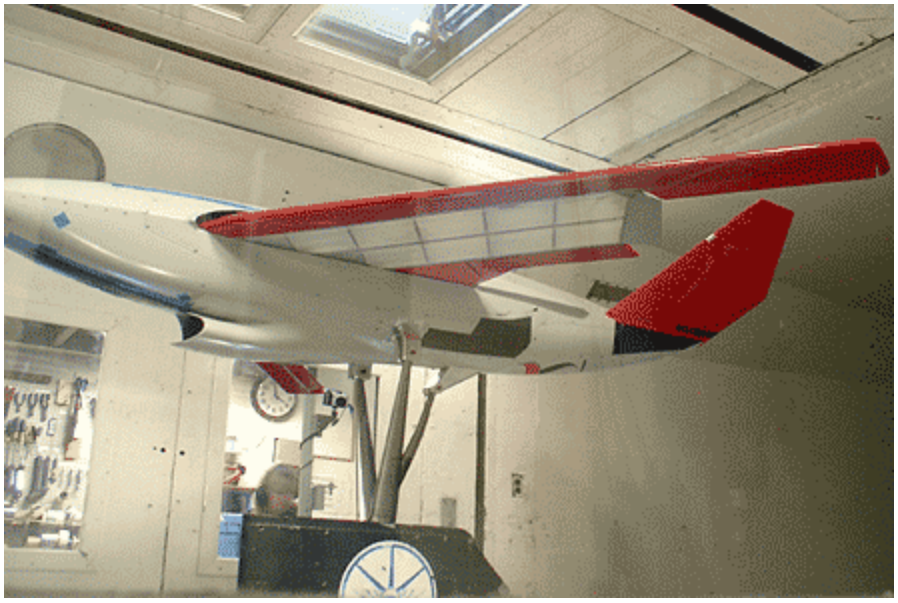

Figure 2.10. NextGen MFX-1 during wind tunnel testing

NextGen went on to start development of the MFX-2, a larger (200 lb.), autonomous, twin engine powered aircraft shown in Figure 2.11. More importantly, its morphing wing setup is larger and has the ability to quickly change shape during maneuvers, giving a potential advantage during possible air combat situations. NextGen claims that the wing is capable of changing surface area by up to forty percent, span by seventy three percent, and aspect ratio by one hundred and seventy seven percent. The MFX-2 successfully underwent five test flights and was able to morph in the air within ten seconds (NextGen, 2008).

Figure 2.11. NextGen MFX-2

3.0 SMART LINK OVERVIEW

The Smart Link design was implemented to demonstrate a morphing structure without using a conventional method such as moving a lockable kinematic mechanism or deforming an elastic structure. Instead, the goal of the design was to use a morphing material that is initially in a hard, immobile state, to soften that material by a stimulus so that its shape can be morphed, and then to re-harden the material to lock the structure in its new position.

The motivation for the Smart Link development came from a morphing unmanned air vehicle (UAV) design proposed by NextGen Aeronautics. Their design utilizes a wing structure where only part of the actual wing volume will morph. This area is closest to the fuselage and is comprised of 6 rigid ribs that will be able to rotate in a fan-like action. Each link sits between two ribs and the morphing action is completed by activating the link and compressing it, causing the entire wing to rotate slightly. In the fully extended state the inner most rib will still be enclosed within the fuselage. This setup is shown in Figures 3.1 and 3.2. The steps of the morphing process can be seen in Figure 3.3. The link is shown in different colors to represent its current state: it is dark blue in the hard state and light blue in the soft state. Rip-stop nylon fabric was used as a skin covering the surface between the ribs, as shown in Figure 3.4. This skin is pulled taut when the links are fully extended and bunches freely when the ribs are collapsed.

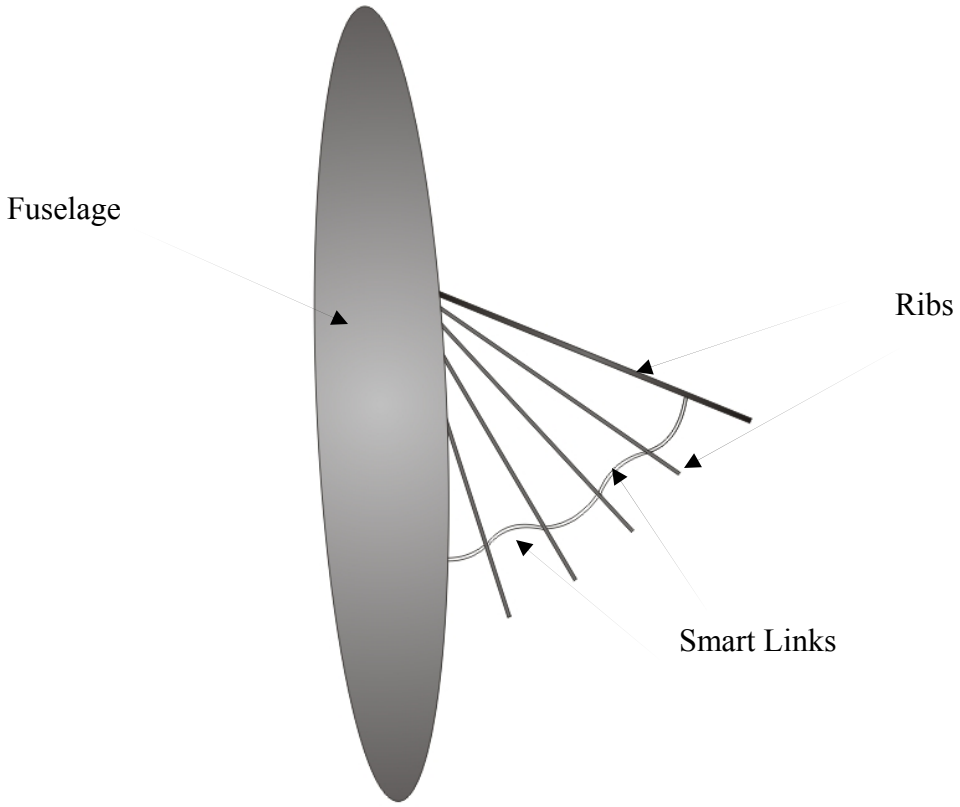

Figure 3.1. Morphing wing schematic without rigid wing section

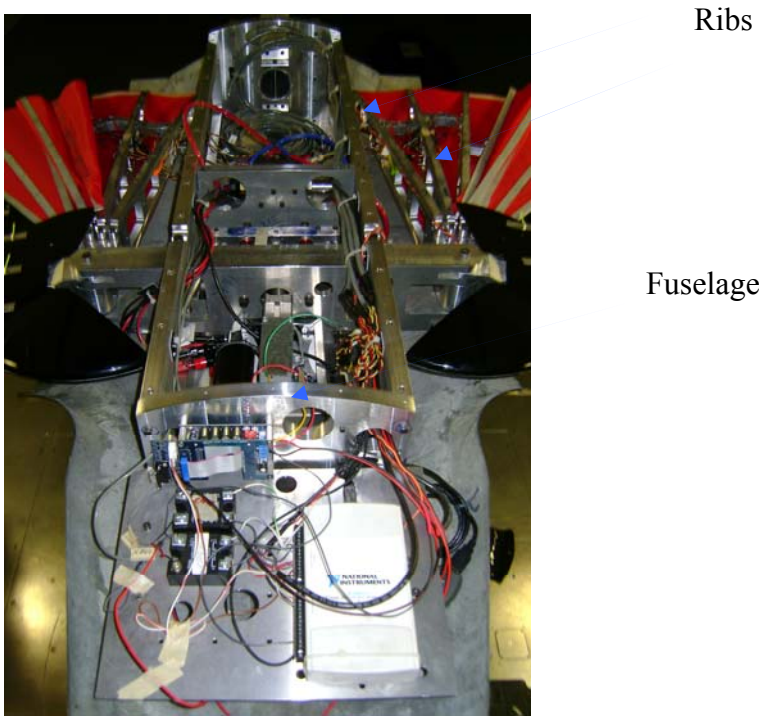

Figure 3.2. Morphing regions of wings with respect to location of the fuselage

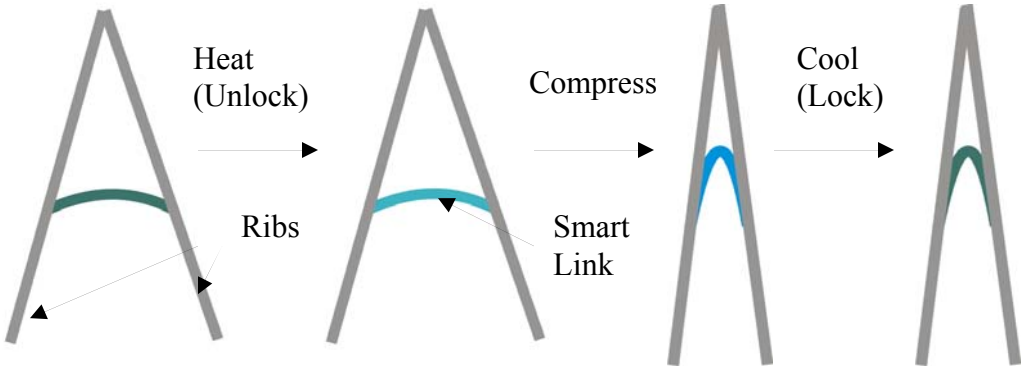

Figure 3.3. Morphing process of single Smart Link

Figure 3.4. Morphing region of fully extended UAV wing (uncovered and covered with nylon skin)

NextGen designed the morphing wing to be partially enveloped by the fuselage. This increases morphing capabilities since wing volume will be able to be decreased by the morphing process and also be tucked away within the fuselage, further decreasing volume and altering aerodynamic properties of the wing. The marriage of conventional hinge technology with novel smart material technology allows the wing to morph to a higher degree without sacrificing overall wing rigidity since only a partial region of the wing is activated to become compliant.

The Smart Link was chosen over a conventional design (which would use a servo motor and a pin-stop) for its simplicity, compactness, and lighter weight. In order to be activated, the Smart Link needs to be heated while a servo controlled hinge design will consist of multiple moving parts and must be properly aligned for locking and unlocking. In comparison, the Smart Link can be activated and locked at any position, allowing for a vast array of morphed configurations. The link is also less bulky and lighter than a servo motor setup which is desirable in flight design. This design is necessary because aerospace designers want to optimize efficiency, and a lighter gross weight will require less lift and less thrust and/or will allow larger payload for the aircraft. A hinge that was controlled by a servo motor and pin setup was

constructed and compared to the Smart Link concept. Figure 3.5 below shows the servo link design.

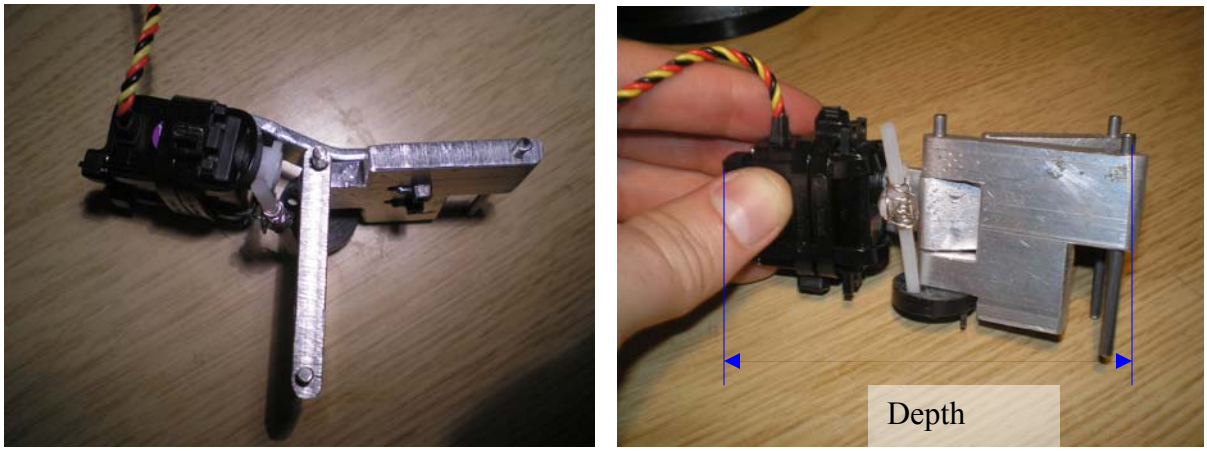

Figure 3.5. Top and side view of Servo Link

In comparison, the Servo Link is much larger than the Smart Link and more than double the size in height (1.8" tall versus a Smart Link height of 0.75"). This added height made it necessary to install the Servo Link further back in the ribs so the link height would not exceed the height of the ribs. The motor is approximately 1.25" deep and contributes to the overall depth of approximately 4". A smaller design is possible but a much more expensive motor is required to offer enough torque for pin placement.

3.1 OUTLINE OF SMART LINK DEVELOPMENT

The initial step in the development of the Smart Link was material selection. Preliminary testing was completed to choose a suitable smart material to use as a locking and unlocking mechanism as well as an elastic material that would serve as the backbone of the link.

Next, the link was designed in accordance with the geometry of the morphing section of the UAV wing. Then, the thermal activation mechanism was chosen to maximize efficiency and

also allow proper movement of the link within the wing. After the design was finalized, a fabrication method for making several links was implemented.

After finalizing the design and producing several links, the link design was tested in the UAV developed by NextGen Aeronautics. This testing was completed in the Kirsten Wing Tunnel on the University of Washington campus with one pair of links (one in each wing in the position closest to the fuselage) being successfully morphed for 3 cycles and an adjacent pair morphed for 2 cycles without significant damage occurring to either link.

3.2 SMART LINK DESIGN REQUIREMENTS

A smart material is used to demonstrate a morphing mechanism orchestrated by a variable modulus material in place of a traditional pinned hinge. In order for this concept to be useable in a practical situation, the link must be able to transition quickly (be able to soften, fold, and then harden rapidly). It must also have enough structural integrity to support the skin tension when in its expanded state, and also to withstand external forces while adjacent links are operated. In other words, the link must have minimal deformation while its neighbors are being compressed or extended. In order to achieve this, it will be highly beneficial to design a link that compresses with low force so that neighboring links remain stationary while the wing section collapses. The link must also be able to start at an interior angle of 130 degrees (pin-to-pin distance of 4.08") and be able to be compressed to an interior angle of 27 (pin-to-pin distance of 1.05"). The interior angle and pin-to-pin distance is displayed in Figure 3.6, where the pins are used to mount the link in the ribs. Lastly, the overall dimensions of the link must be chosen so that there is no interference with the ribs during any part of the morphing cycle. The slots in the ribs are

approximately 0.8125 inches high, so the link must be able to slide through as the SMP bulges during compression. A partially collapsed link within a rib slot is shown in Figure 3.7.

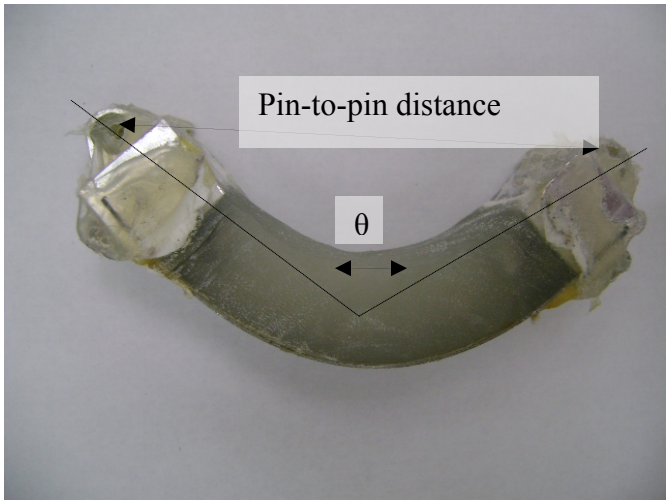

Figure 3.6. Interior angle and pin-to-pin distance of Smart Link

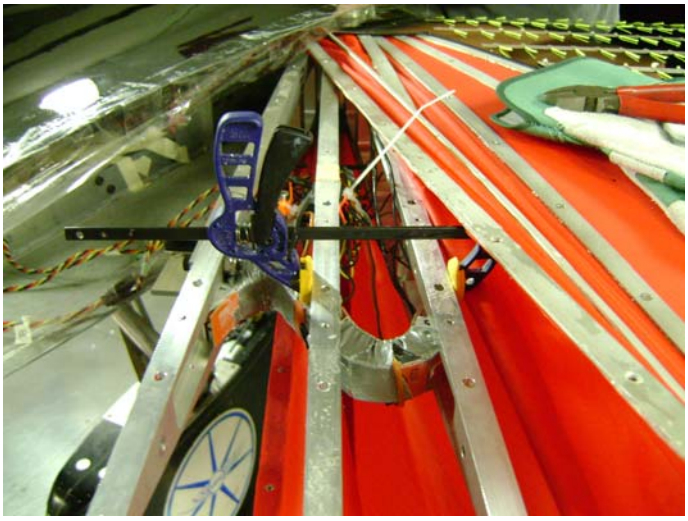

Figure 3.7. Partially collapsed links within rib slot

Explicit tolerances for link deformation in the hard state due to external forces are defined so that the exposed skin covering the morphing wing portion will not sag unnecessarily. These tolerances, provided by NextGen, include no more than 2 degrees of inner angle deflection when the link faces a compressive force in the hard state due to its neighbor being collapsed in

the soft state. It was also decided that the link had to withstand this same force while hardened in the collapsed state with less than 2 degrees of inner deflection in compression and tension. This was decided because the link will experience a tensile force while its neighbors are fully expanded until the nylon skin is tightened. This force was unknown since the wing was not yet built and a force of 100 lbf was used as the maximum required load for link collapsing in the design.

The next major design specification when considering the Smart Link design was activation time. NextGen initially suggested a thermal transition time of less than 10 seconds for link activation. This specification will be important when decided what smart material to implement and what device to use for material activation.

In order for the polymer to transition as quickly as possible, a very high temperature gradient between the heating element and polymer is required. However, since the maximum temperature of the SMP will be the limiting factor, activation time for a given cross section can only be made so low due to the physical properties of the polymer. A more thorough theoretical approach to quantifying thermal activation time is shown in Chapter 5.

3.3 SMART LINK DEVELOPMENT PHASE I

After taking design specifications into consideration, materials were chosen that would best suit the morphing scenario. Shape memory polymer was chosen due to its ability to be easily altered into a new configuration and be hardened or locked in place. The first concept of the link employed SMP so that the link could be transitioned from hard to soft to allow shape change. On either side of the SMP volumes, rigid members are connected to an elastic

backbone. This link would bend in plane and be capable of returning to its original position due to the elastic backbone. The link would be totally rigid when the SMP sections are hard and flexible when soft with independent SMP volumes to control the direction of deflection. This concept is shown in Figure 3.8

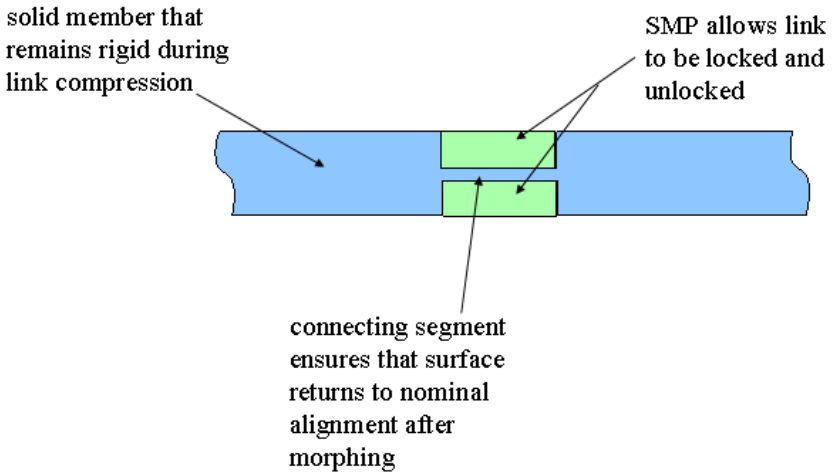

Figure 3.8. Smart Link concept with two variable stiffness regions

The initial design would be operated in the following manner: one of the two SMP volumes would be thermally activated and softened, a small initial force would be applied to initiate bending in a desired direction, and then, the remaining SMP volume would be softened to allow free bending in the polymer joint. After bending, the SMP would be allowed to cool and lock the link in its deformed position. This process is displayed in Figure 3.9.

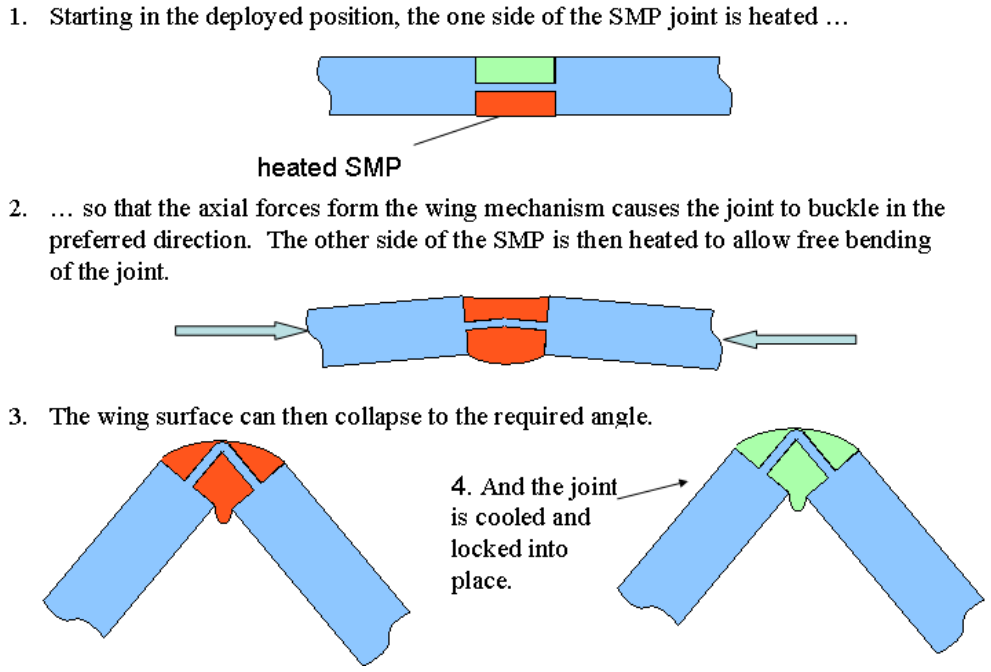

Figure 3.9. Operation of initial Smart Link concept

Veriflex, a commercially available shape memory polymer designed and sold by CRG Industries, was chosen for the design due to its relatively low activation temperature (62 °C) and robust mechanical properties shown in Table 1. Also, this was the polymer utilized by Rauscher (2008) in a morphing tile design and its morphing capabilities were well documented in a quantitative form.

Table 1. Mechanical properties of Veriflex (CRG Industries, LLC, 2005)

Property	Specification (T<Tg)
Tensile Strength	22.96 Mpa
Tensile Modulus	1241.05 Mpa
Elongation to Break	3.90%
Flexural Strength	31.72 Mpa
Flexural Modulus	1241.05 Mpa
Compressive Strength	32.41 Mpa
Compressive Modulus	1447.90 Mpa
Thermal Conductivity	0.17 W/(m*K) at 18.6 deg. C
Density	920 kg/m^3

Young's modulus values for thermally activated Veriflex are shown below in Table 2. The activated moduli values are approximately 4 orders of magnitude lower than in the hard state, making Veriflex a suitable candidate for the locking (hardening) and unlocking (softening) scenario experienced in the wing.

Table 2. Young's Modulus values for Veriflex determined experimentally (Beblo, 2008)

Axial		Transverse	
T<Tg	T>Tg	T<Tg	T>Tg
23 °C	80 °C	23 °C	80 °C
1050 Mpa	0.24 Mpa	1050 Mpa	0.24 Mpa

A uniform piece of aluminum was first tested to see if it was capable of large deflection without exceeding its elastic limit. Aluminum was chosen due to its low density and relative lack of stiffness when compared to other metals. This initial design without the shape memory polymer regions is shown in Figure 3.10.

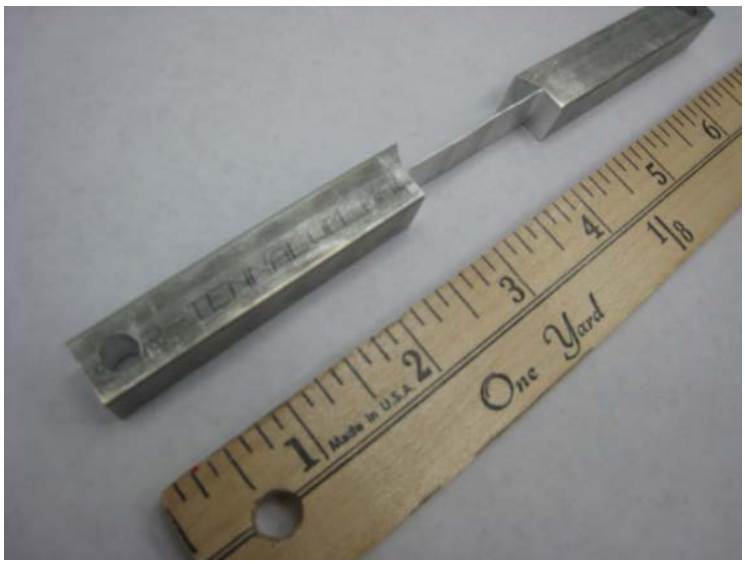

Figure 3.10. Initial continuous link without SMP

This test was completed in an MTI 5K load frame, as shown in Figure 3.11. A pin-pin setup was used when testing the link, with each clamp holding two strips of aluminum that secured the pin.

Figure 3.11. Continuous aluminum link without SMP in load frame

The test proved that the continuous aluminum link was not capable of being compressed fully and returning elastically. This is undesirable since continued cycles of plastic deformation will eventually lead to failure.

Next, a composite structure was developed. Aluminum was used for the rigid end clamps and 301FH spring steel was implemented for the flexible mid-section, as shown in Figure 3.12. However, unlike the continuous aluminum design, the spring steel was moved toward one side. This layout helps to prevent the SMP from delaminating from the flexing surface since none of the SMP will actually be in tension during activation and bending. Also, bolts were added on the inner sides of the aluminum members to prevent polymer delamination on these sides. The separation was prevented because the polymer would cure around the heads of the bolts,

providing a stronger bond than simple adhesion to the flat aluminum clamps surfaces. These bolts can be seen in Figure 3.15.

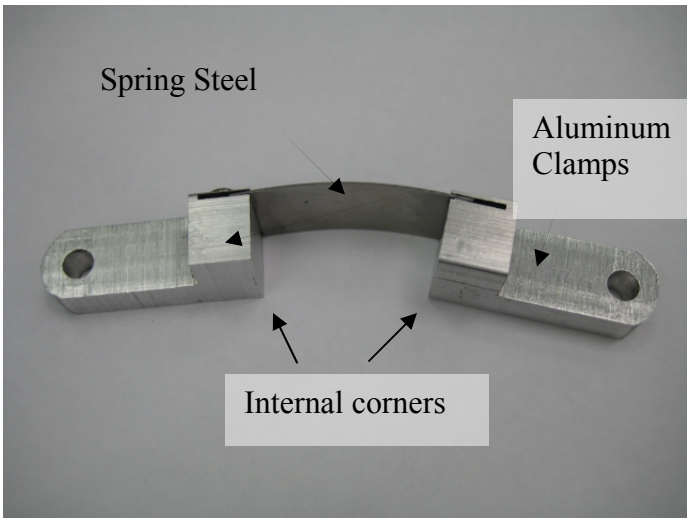

Figure 3.12. Initial continuous link without SMP

Load frame testing was performed on this link design. The spring steel section did not yield severely like the aluminum, but was still unable to return to the initial position. It was also noticed that the SMP region was relatively short when compared to the overall length of the link and this caused extremely high compression within the polymer. In fact, the internal corners of the structure came close to making contact when the link was fully compressed (location of corners shown in Figure 3.12). Out of plane buckling of the SMP ensued due to the vast decrease in volume between the aluminum members. The extreme stress experienced by the shape memory polymer caused rupture. Buckling and rupturing of the polymer region are shown in Figures 3.15 and 3.16. Thermal cycling was achieved during the testing process by securing the links within the load frame clamps, heating the environmental chamber until the polymer was fully softened, and applying a load to compress the link. The chamber was then cooled to allow the polymer to harden in this configuration. After complete hardening, the chamber was heated

again and the polymer was activated fully. The compressive load was then removed to extend the link to its initial configuration. The load frame setup used for thermal testing is shown below in Figure 3.14.

Another design was also tried with multiple layers of spring steel, shown in Figure 3.13. This design did not work because the added spring steel added too much stiffness for the link to deform under a reasonable load, and when the link would deform, plastic deformation was likely to occur within the steel.

Figure 3.13. Smart Link with additional spring steel elements

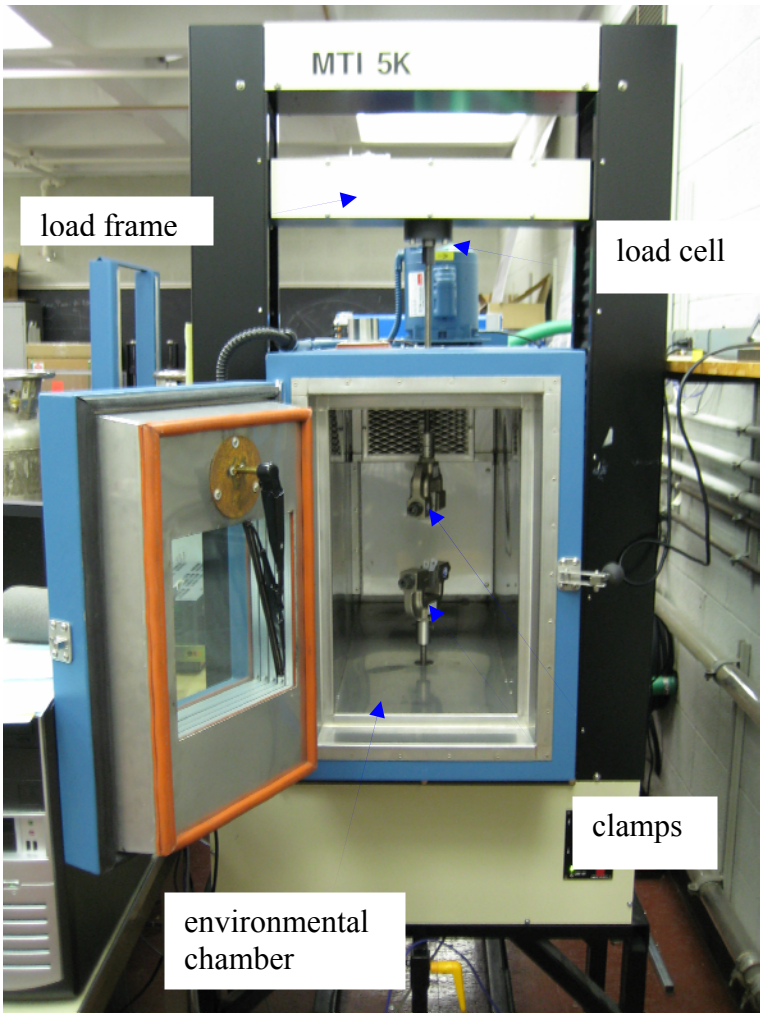

Figure 3.14. Load frame setup for thermal testing of Smart Link design

Figure 3.15. Ruptured SMP after thermal cycling and compression

Figure 3.16. Buckling of SMP during compression test as link bends away from camera view

3.4 SMART LINK DEVELOPMENT PHASE II

Further development of the Smart Link involved addressing the problems of polymer bulging and failure and plastic deformation of the bending element. The volume of SMP within the link

was extended in order to alleviate stress significantly. Compressive testing showed that this remedy did in fact solve the problem of polymer failure. The problem of plastic deformation during bending was also resolved by implementing a nitinol member in place of the spring steel. Nitinol enabled the link to bend to an extent where the aluminum clamps would touch without causing plastic deformation in the backbone and made the link capable of self expansion since the nitinol member's initial configuration was flat at 180 degrees.

The next step in design involved choosing a method of thermal activation. The heating method, whether internal or external, must be capable of fitting within the wing assembly, of thermally transitioning the link in an acceptable time, and also not prohibit the deformation of the link.

Internal heating was initially chosen so that there would be no additional material surrounding the link to interfere with the fan ribs. More specifically, a coil of nichrome wire was placed in the middle of the SMP region. This setup is shown in Figure 3.17.

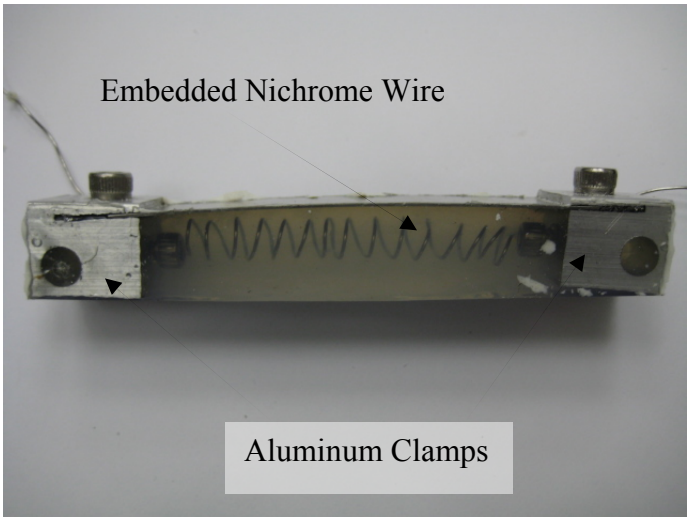

Figure 3.17. Smart Link setup with nitinol flexural member and internal nichrome heating coil

Thermal testing revealed that the coil was capable of transitioning the majority of the polymer region, but failed to activate the regions closest to the aluminum clamps due to the heat

sink characteristics of the aluminum. This created a scenario similar to the phase I design, where a smaller transitioned polymer region equated to greater stress and eventual rupture.

Testing was completed in two scenarios to determine the cause of rupturing. While the entire SMP region was not activated and this may have caused failure, the introduction of the coil into the polymer altered the bending response of the link. In order to discern what aspect was the cause of failure, the link was activated in two separate ways: heating with the inner coil and heating externally in an environmental chamber.

Internal heating was performed while the link was constrained from movement during the process of thermal activation. It was deformed after the SMP softened, then clamped into position and allowed to cool. The clamp was then removed and the link would slowly reverse position by about a tenth of an inch due to the stored strain energy within the nitinol. To complete the thermal cycle, the link would be clamped again and the nichrome coil would be electrified. However, after reaching partial activation in the locked position, the middle region of SMP would begin to cloud. Upon extension, the polymer began to rupture and rip apart, as shown in Figure 3.18. It is not clear why the clouding and rupturing occurred, although it appears to be a permanent change in material properties, possibly due to the combination of high heat and stress.

Figure 3.18. Failure of SMP during nichrome activation

During coil heating operation the internal temperature was monitored using a Type K thermocouple. This thermocouple was glued onto the nichrome coil and monitored to ensure that the coil was not exceeding a temperature of 135 degrees Celsius and changing mechanical properties of the polymer. While this appeared to hold true when the link was in its extended configuration (no damage was done to the SMP in that case), it is not clear that polymer degradation did not occur in the compressed configuration, even though the temperature did not exceed 135 degrees.

External heating was then tested for comparison against the nichrome coil. An identical link to the one described above (with heating coil, but unused in this case) was tested. The external thermal cycle started by setting the initial configuration to an inner angle of 130 degrees. The link was then clamped so that it would not expand until thermal transition was completed. Next, the environmental chamber was set at 100 degree C and the link was allowed transition fully. The link was then compressed and removed from the chamber and cooled until the polymer was fully hardened. The clamp was removed to ensure that the link was fully hardened and would retain its shape. At this point the link extended similarly to the heating coil case due to stored energy within the bent nitinol (approximately 0.1 inches). The link was then clamped

and returned to the hot chamber until full transition. Upon extension, the polymer did not discolor, rupture or fail. These results suggest utilizing internal heating will require a more intricate and costly approach than the simple coil that was employed in our testing, while external heating can transition the polymer well enough for link operation without failure.

Lastly, the configuration in which the polymer was poured and cured was changed from 180 degrees to various angles. Starting in a pre-deformed shape requires less compression within the SMP region during deflection and lowers the force needed for compression. A tradeoff was needed, however, to allow the link to be expanded to the design specification of 130 degrees without ripping apart the polymer or causing it to pull apart from any of the interfaces. Initial angles of 80 and 95 degrees (various angles between full extension and full compression within the fan ribs) were tested and it was found that 95 degrees was the best angle because the 80 degree configuration caused separation at the polymer and frame interface after full extension.

4.0 LINK ACTIVATION METHODOLOGY AND DESIGN

A variety of external heating methods were considered in the finalized Smart Link design. Commercially available heating devices included heating tape (a long, narrow, pliable electric coil wrapped in fabric shown in Figure 4.1), nichrome wire, and pliable silicone heating pads with a wire coil on the inside. For wind tunnel testing, an external power supply was utilized so power consumption for a single active link was no concern. However, activating more than one link at once could possibly draw very high current, and this was one criterion used when selecting the proper heating device. Power supplies were selected that were capable of producing 10 A at 10 V, so a device had to be chosen that would not exceed these limits even if 2 were operated simultaneously.

Figure 4.1. Smart Link wrapped with heating tape

The foremost goal when considering thermal design of the Smart Link is time required for one complete thermal cycle. Factors affecting transient thermal response include size constraints and active heated surface area. Since the link must bend to extreme measures, the most practical setup in a static case may not be suitable in bending within the morphing rib setup due to interference or constraints caused by the heating element.

In order to optimize link activation time, the surface area of the SMP that is covered by the heating device must be maximized. For heating, ideally all of the surface area would be covered so that heat would not only enter the polymer, but also not escape into the ambient surroundings. However, covering the entire polymer with a heating element decreases the rate that heat can escape and will lengthen the cooling process considerably. Heating the link exceptionally fast but cooling it very slowly will not be beneficial because the full heating and cooling cycle must occur during the wing morphing process. The thermal design of the link will require a solution that can heat the polymer in a reasonable time but also not cover the link fully so cooling is efficient as well.

The size of the external heater also governed the selection. The slot cutout in each rib for the link was approximately 0.8125 inches tall. This was a limiting dimension since the thick heating tape would interfere with the slot as the link was collapsed. Implementation of the tape also brought another aspect into consideration: interference with respect to maximum allowable deflection. As can be seen in Figure 4.1, the tape adds considerable thickness to the Smart Link and prevents complete closure. It also adds considerable stiffness (since it must be wrapped tightly to keep constant physical contact with the link) and makes the design more cumbersome since it has a tendency to unwrap.

Nichrome wire was then considered as a candidate for external heating. In order to preserve some flexibility, the wire would need to be wrapped in a spiral around the link. Initial testing showed that the wire was not capable of fully transitioning the polymer region. This was due to the limited surface area of the wire that was in contact with the link. The test was completed with aluminum foil wrapped around the link and the nichrome wire spiraled around the foil. This was done to increase heat dispersion around the link but was not sufficient since the wire could not get hot enough for rapid heat transfer without oxidizing the SMP.

Commercially available silicone heating pads were the next method tested. These pads, shown in Figure 4.2, are held flush against the sides of the link using adhesive tape. This tape is wrapped loosely, allowing the pads to slide against of the surface of the link during bending without adding substantial stiffness (shown in Figure 5.1). Thermal grease was added at the interface between the pads and SMP and between the pads and the nitinol to increase heat transfer and decrease friction. Figure 4.3 displays a heating pad placed onto the nitinol side of the link.

Figure 4.2. 3 inch long silicone heating pad trimmed to approximately 0.71 inches high

Figure 4.3. Silicone pad butted against nitinol side of Smart Link

It is possible to model the heating pad design using one dimensional heat transfer analysis without exterior heat loss. This best-case-scenario approach is useful when choosing if a thermally activated smart material (SMP in this case) is practical for the given application. In other words, if a transition time of 10 seconds or less is required, and the optimal theoretical model predicts 5 minutes, then no amount of thermal design will be able to satisfy the design requirement. This optimal scenario, shown in Figure 4.4, consists of a solid slab that is infinitely long and tall, so that heat will only travel in the width or z dimension. This scenario also assumes no heat loss to the surrounding environment, which will make transient heat response more efficient.

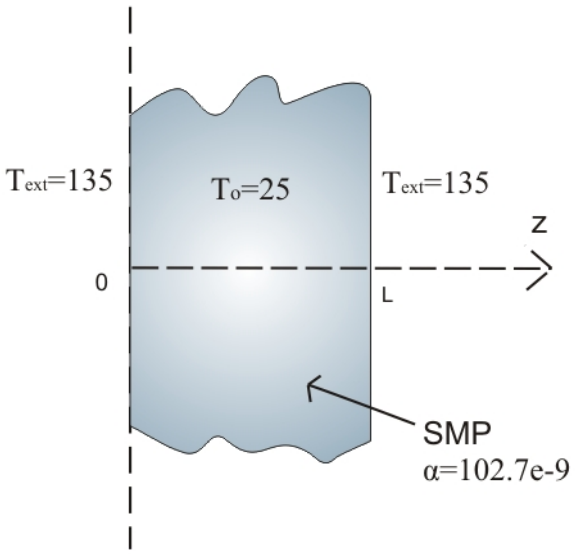

Figure 4.4. One dimensional heat transfer schematic

The optimal theoretical model was constructed using a one dimensional approximation of the heat equation. The governing formulation of this concept is shown in Equation 1 (Özişik, 1985).

$$\frac{\partial^2 T(z,t)}{\partial z^2} = \frac{1}{\beta}\frac{\partial T(z,t)}{\partial t} \qquad in\ 0 < z < L,\ t > 0 \tag{1}$$

with the boundary conditions

$$\begin{aligned} T(z,t) &= 0 \quad at\ z = 0, t > 0 \\ T(z,t) &= 0 \quad at\ z = L, t > 0 \end{aligned} \tag{2}$$

and the initial condition

$$T(z,t) = F(z) \quad for\ t = 0, in\ 0 \le z \le L \tag{3}$$

While the actual temperature values on the boundary are 135 degrees, they are modeled at 0 degrees to coincide with the theoretical model. This difference was taken into account by

changing the initial interior temperature by an offset of -135 degrees, making it -110 degrees in the model. The results were then compensated by increasing all temperature values by 110 degrees. This will not introduce error since all physical properties are assumed to be constant throughout all temperature values.

One of these values, the thermal diffusivity, was referenced from Gross (2008) and its value is shown in Equation 5, where

$$\kappa = 0.17 \frac{W}{m * k}$$
$$\rho = 920 \frac{kg}{m^3} \tag{4}$$
$$C_p = 25 \frac{J}{kg * K}$$

and

$$\beta = \frac{\kappa}{\rho C_p} = 102.7 * 10^{-9} \frac{m^2}{s} \tag{5}$$

Separation of variables, shown in Equation 2, is then utilized for a solution method.

$$\frac{Z''(z)}{Z(z)} = \frac{\Omega'(t)}{\beta^2 \Omega(t)} = -\lambda^2 \tag{6}$$

where

$$Z''(z) + \lambda^2 Z(z) = 0 \tag{7}$$

and

$$\Omega'(t) + \beta^2 \lambda^2 \Omega(t) = 0 \tag{8}$$

Equation 8 is an ordinary differential equation and its solution can be expressed as shown in Equation 9.

$$\Omega(t) = e^{-\alpha \lambda^2 t} \tag{9}$$

The solution to Equation 7 can be written as

$$Z(\lambda, z) = C_1 \sin(\lambda z) + C_2 \cos(\lambda z) \tag{10}$$

Which, due to the boundary conditions, is represented as

$$Z(\lambda, z) = C_1 \sin(\lambda z) \tag{11}$$

where

$$\sin(\lambda L) = 0 \tag{12}$$

and

$$\lambda_n = \frac{n\pi}{L} \quad n = 1,2,3,\ldots \tag{13}$$

The overall solution is then assumed to be the product of the separated solutions, shown in Equation 14.

$$T(t)Z(\lambda_n, z) = e^{-\beta\lambda_n^2 t} \sin(\lambda_n z) \tag{14}$$

The finalized solution for temperature is then displayed as a sum of all individual solutions and is shown in Equation 15.

$$T(z,t) = \sum_{n=1}^{\infty} C_n e^{-\beta\lambda_n^2 t} \lambda_n z \tag{15}$$

The initial condition for the model is shown in Equation 16 and is chosen to coincide with the physical scenario in the morphing wing setup. A temperature of 135 degrees is chosen since it is the maximum temperature that the SMP can experience without oxidation. The silicone heating pads were controlled so not as to exceed this temperature in the test setup.

$$T(z,t) = 135 \quad for\ t = 0,\ in\ 0 \le z \le L \tag{16}$$

The final formulation of the temperature distribution of a function of location and time is shown below in Equation 17:

$$T(z,t) = \frac{4T_o}{\pi} \sum_{n=1,3,5\ldots}^{\infty} \frac{1}{n} e^{-\beta(n\pi/L)^2} \sin\left(\frac{n\pi z}{L}\right) \tag{17}$$

where T_o is the initial internal temperature of the slab and L is the width of the slab.

The middle section of the slab at $\frac{L}{2}$ is of most interest for transient analysis since it will be last to reach steady state. The transient response, shown in terms of time and position in Figure 4.5 and time and position at the middle in Figure 4.6, shows that the mid-section reaches the activation temperature of 62 degrees Celsius at approximately 175 seconds. Matlab code accompanying this model is displayed in Appendix B. This response greatly overshoots the design specification of an activation time of 10 seconds or less. It is important to note that the model does *not* include the nitinol layer. Adding the nitinol layer into the model would slightly increase the time required for activation. Even though it will be able to dissipate heat faster than the polymer, it will also add to the total distance that the heat needs to travel through. These results prove that in a real world situation with one dimensional heat transfer (two heating pads sandwiched on opposite sides of the link), the polymer is not physically capable of transitioning any faster while using the silicone heating pads, even if heat loss is kept to a minimum. More creative heating methods utilizing different boundary conditions (such as surrounding the entire area of polymer with heating elements or using a form of heat transfer other than conduction) may be able to activate the polymer faster.

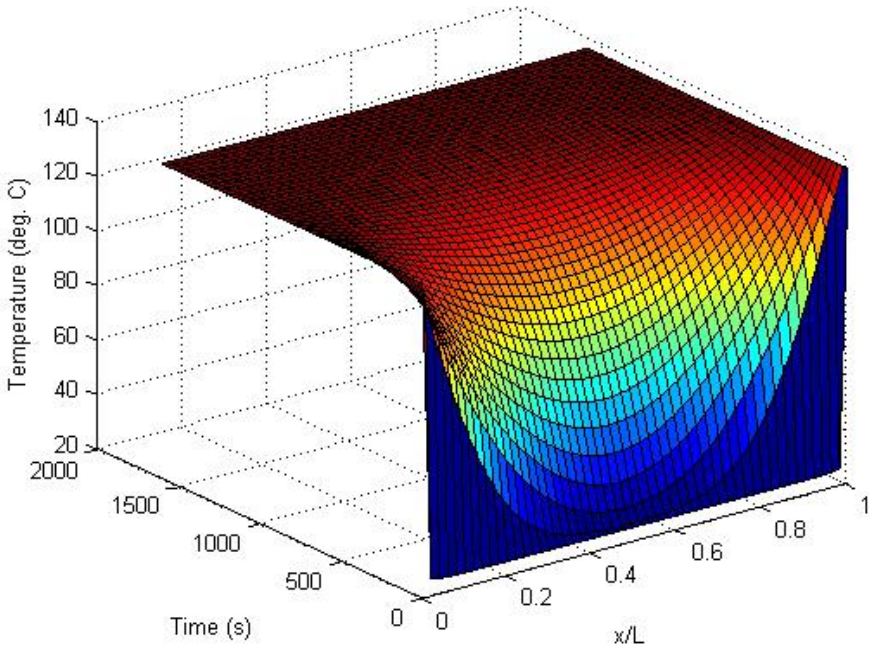

Figure 4.5. Transient response of entire width of SMP during activation

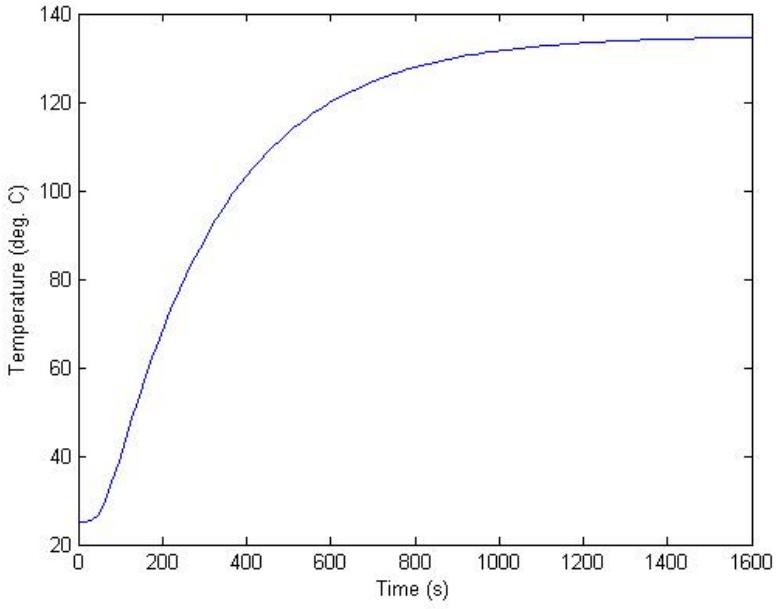

Figure 4.6. Transient response of middle section of SMP during theoretical activation

5.0 FINAL SMART LINK DESIGN

The final Smart Link designed was comprised of a member that consisted of two aluminum side clamps, a nitinol backbone, shape memory polymer core, silicone heating pads taped on the front and back, a thermocouple glued onto the middle of the top of the polymer, and a plastic bushing in the pin hole on both clamps. This final link is shown in Figure 5.1.

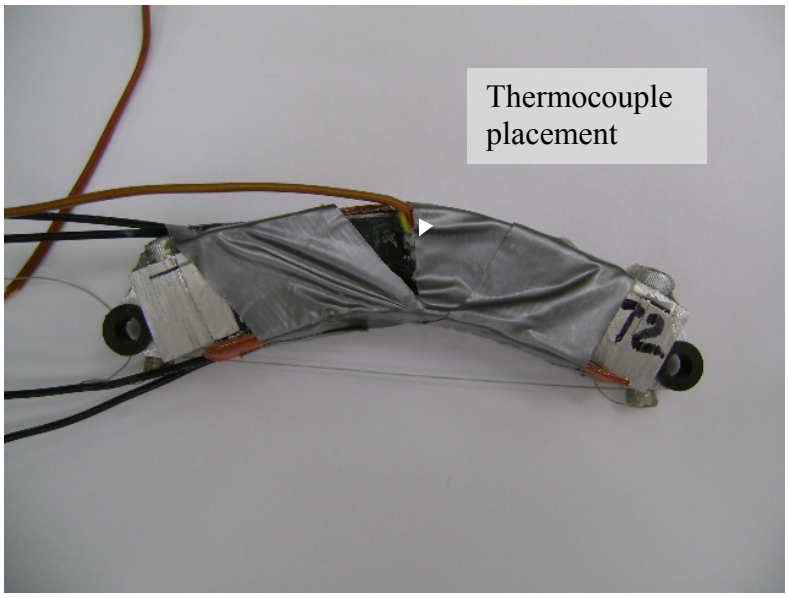

Figure 5.1. Final assembly of Smart Link

The dimensions for the composite cross section are shown in Figure 5.2. The pin-to-pin arc length (pin-to-pin distance if the link was flattened) of 4.5"

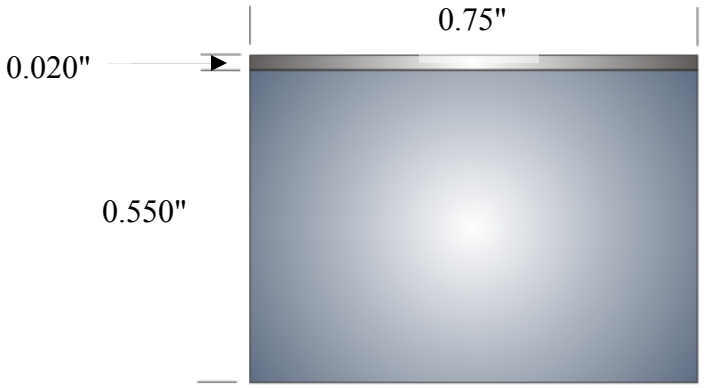

Figure 5.2. Dimensions of polymer and nitinol cross section in Smart Link

Two thermocouples were used to monitor heating of the link in the aircraft. One thermocouple was placed on the top and middle of the SMP because this will give a conservative temperature estimate at the middle of the polymer. It was found that when this thermocouple read 65 degrees Celsius the majority of the polymer was transitioned and the link could be effectively compressed. Testing also revealed that when the temperature measurement approached 40 degrees Celsius on the cooling cycle the compressive load could be removed from the link without significant spring-back or damage to the polymer. The second thermocouple was placed under the heating pad (between the heating pad and the nitinol layer) to ensure that the temperature did not exceed 135 degrees Celsius.

Plastic bushings were utilized in the design to reduce friction within the pin holes of the clamps. The links would be installed so that the pin would be hammered through holes in the rib (making a press fit), requiring minimal friction on the pin-link interface for optimal performance. This location of the press fit pin holes is shown in Figure 5.3. As the ribs extend, the pin stays stationary in the rib and the link rotates around the pin. If friction was significant between the link and pin, greater actuation force would be required to move the ribs and this would impose

greater stress within the link. Also, the final design of the aluminum clamps involved rounding off the far edges of the clamp to allow full rotation around the pin without interfering with an adjacent link.

Figure 5.3. Location of press fit holes in rib and bushing in link

Some additional changes were made on the link to assure proper performance during wind tunnel testing. The heating pads were trimmed to a height of 0.71 inches to assure that there would be no interference within the rib due to polymer bulging and the added height due to the adhesive tape. Also, part of the polymer was ground away to prevent bulging interference of the polymer area that was directly enclosed within the rib. This ground area is shown in Figure 5.4.

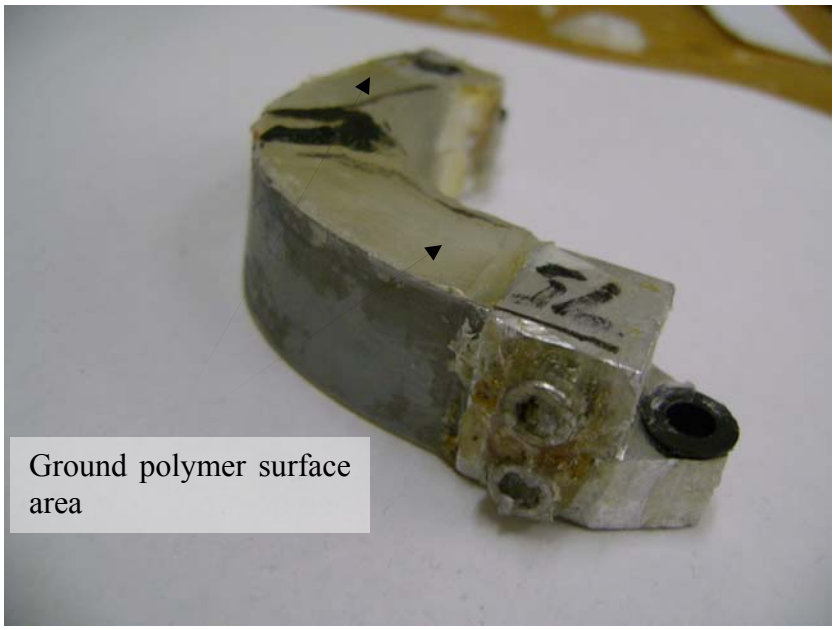

Figure 5.4. Surface area where SMP was ground away to prevent interference with ribs

6.0 SMART LINK FABRICATION

The fabrication of the final design of the link was completed in two processes: machining the aluminum clamps and the nitinol and pouring and curing the Veriflex shape memory polymer within the link structure. 6160 grade aluminum was chosen for the clamps due to its ease of machinability.

The link frame was set up as a mold for the liquid shape memory polymer to be poured into. The links were secured to a wooden board with screws and aligned so that this configuration produced an interior angle of 95 degrees, as shown in Figure 6.2. Thick aluminum foil was then placed in the front and back (nitinol) side of the link to act as a dam for the liquid polymer. Silicone sealant was applied to all interfaces that were not watertight to prevent polymer leakage during the cure cycle. The polymer was then poured slightly higher than the height of the link since slight shrinkage occurs while curing.

The liquid Veriflex is prepared by mixing a liquid resin with a liquid hardener in the ratio of 24:1. This proportion is mixed thoroughly and exposed to a vacuum environment to remove small air bubbles introduced during mixing. This vacuum setup, shown in Figure 6.1, is pumped down to a vacuum pressure of 27 in. Hg. The vacuum is held for 30 seconds and then released to prevent styrene (present in the resin) from being extracted in the form of a gas. This vacuum cycle was completed 3 times or until visible bubbles were minimized.

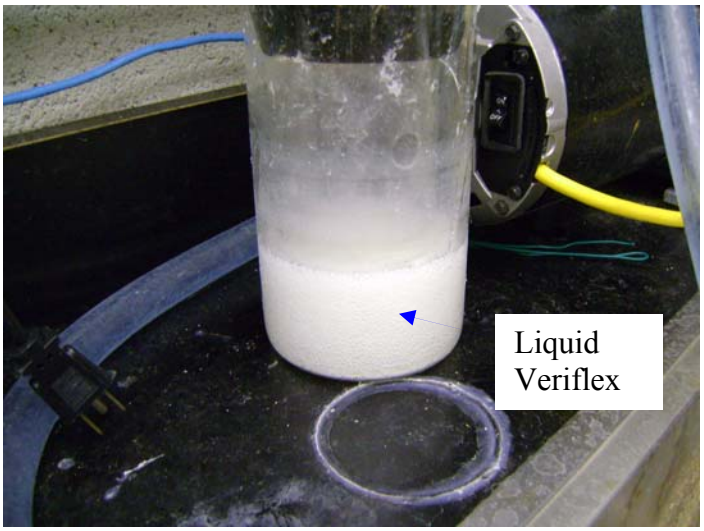

Figure 6.1. Mixed Veriflex under vacuum conditions

After the curing process is complete, the links are removed from the board and the aluminum foil is pulled away. Any remaining silicone sealant is cut away and the excess polymer that is a resultant of the over-pour is ground away to create a flat surface flush with the nitinol. The finalized link is shown in Figure 6.3.

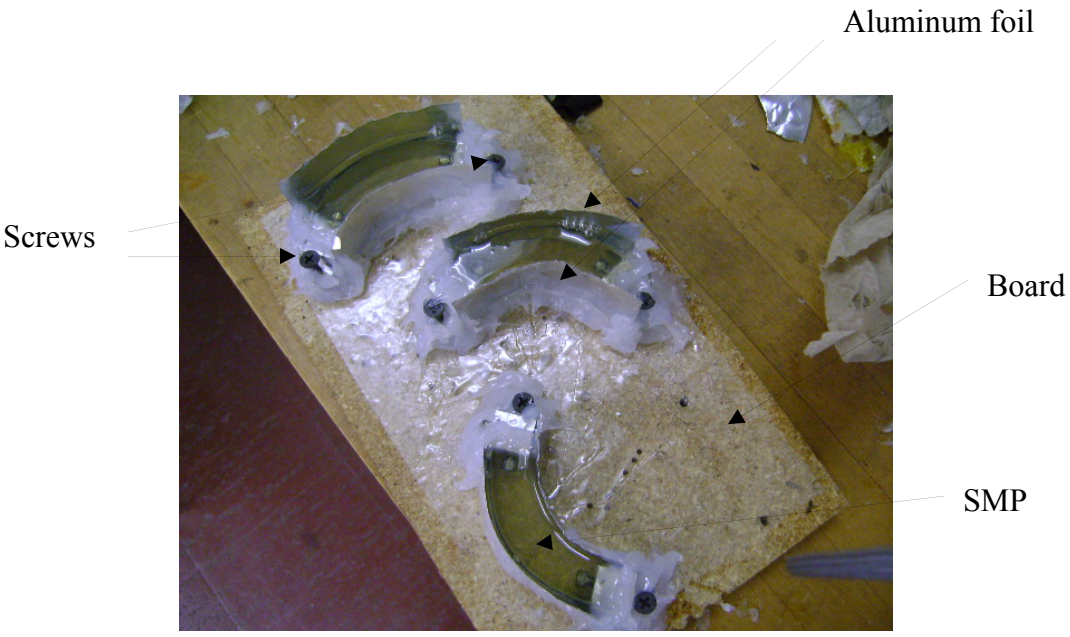

Figure 6.2. Smart Links at 95 degree initial interior angle after curing process is complete

Figure 6.3. Final Smart Link after fabrication process

7.0 THEORETICAL ANALYSIS OF DEFLECTION

A theoretical model was constructed for use as a future design tool. This model considered the case when the SMP was activated and fully compliant with the nitinol contributing to the majority of the stiffness. Results from this model were useful because the results can be used to base the actuator selection. This selection is important because a massive actuator will add surplus weight to the aircraft and hinder performance. A theoretical model will also allow the designer to minimize the force so that adjacent hardened links will not be deformed while its neighbor is actuated.

7.1 DEFLECTION MODEL FORMULATION

A model composed by González and LLorca (2004) was considered for use when modeling the Smart Link. This representation analyzes a pre-curved elastic beam with constant radius of curvature and an axial tensile load imposed on the tip. Their theory also includes the effects of large deformation and extensibility. However, the derivation of the link model will be considered inextensible since the main contributor of stiffness, the nitinol strip, will deform little in the axial direction during bending. A schematic of the scenario defined by González and LLorca is shown in Figure 7.1.

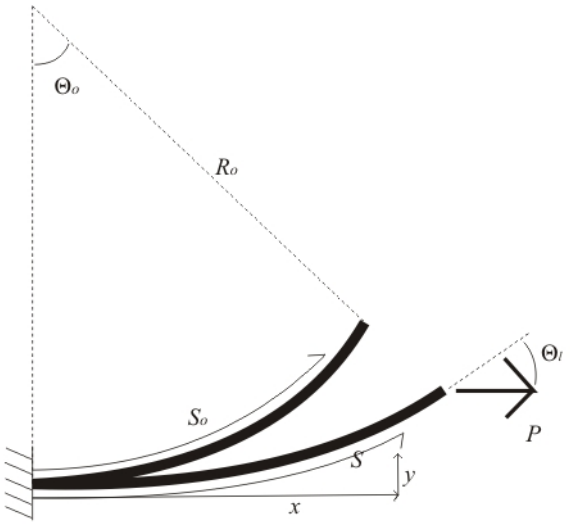

Figure 7.1. Curved beam in initial and deformed configurations

A number of assumptions were made when constructing the model. First, symmetry was used to analyze the pinned-pinned link structure as a cantilevered beam with a load that is always horizontal. Also, since the initial configuration of the nitinol member is flat, the initial radius of curvature, R_o, was set very high to approach infinity (set to $1*10^{33}$). This was decided because a beam with an exceptionally high radius of curvature will behave similarly to a beam with no curvature once bending ensues. A parametric study was completed to see at what large value of initial radius of curvature the deflection would converge to approach the behavior of a straight beam. Figure 7.2 displays the angular tip deflection (Θ_o) for initial radius values of 2.5, 10, and 1e33 inches. The deflection behavior, sufficiently past initial bending, shows that the difference between the radius values of 10 and 1e33 inches is minimal and it can be assumed that deflection behavior reaches convergence at a radius value of 1e33 or less. Also, since the link will never experience an interior angle larger than 130 degrees, the beam will never actually be flat, so buckling is of no concern.

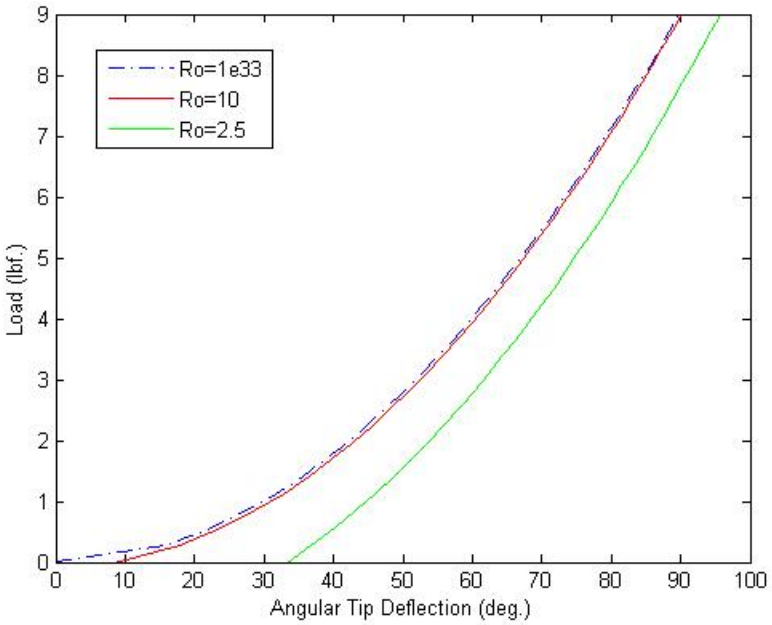

Figure 7.2. Parametric comparison of varying initial radius of curvature

Next, it was assumed that the polymer and nitinol both possess the same initial radius of curvature under equilibrium with no applied load. This is not physically realistic since the polymer is poured at an interior angle of 95 degrees and not 180 degrees. However, this difference was considered negligible while the polymer was thermally activated since it has a Young's modulus of only 29 psi and 4 orders of magnitude lower than the nitinol. If both materials were equally stiff, then their initial, unloaded radii of curvature would have to be equal for the model to be accurate.

The next assumption involved the traditional dimensions of a slender beam using Bernoulli-Euler beam theory. These dimensions state that a long, slender beam is generally 10 times as wide as it is thick and 10 times as long as it is wide. The dimensions of the polymer region are 0.75" by 0.55" and violate the dimensions of a traditional beam. However, since the polymer is 4 orders of magnitude softer than the nitinol member, it was believed that the

mechanics of the nitinol would dominate the response. The width to length ratio of the nitinol member did not match up either, with the width being 0.75" and the length being 1.28".

Another major assumption was that the nitinol was fully transitioned to martensite throughout the entire process of deformation. This assumption will be a source of error since the exact martensitic fraction was not taken into account and any present volume in the austenite phase will cause greater stiffness. This assumption was made since the final state of deflection is of most interest when using the model as a design tool and the martensitic fraction will be at its greatest at full deflection.

In the formulation, any variable with the subscript 'o' refers to the initial configuration. $1/R_o$ is the initial curvature of the entire beam and the beam has a length of $2l$. González and LLorca define the force as axial in the positive x-direction, but the Smart Link experiences a compressive force in the x-direction, so the force will be in the opposite direction of what is seen in Figure 7.1.

According to Bernouilli-Euler beam theory, the curvature of the beam is given by

$$\frac{d\Theta}{ds} = \frac{1}{R_o} - \frac{-P\left[y(l) - y(s)\right]}{EI} = \frac{1}{R_o} + \frac{P\left[y(l) - y(s)\right]}{EI} \tag{18}$$

where E is Young's Modulus and I is the second area moment of inertia of the cross section of the beam.

Differentiating Equation 18 yields

$$\frac{d^2\Theta}{ds^2} = \frac{-P}{EI}\frac{dy}{ds} = \frac{-P}{EI}\sin\Theta \tag{19}$$

where

$$\frac{dy}{ds} = \sin\Theta \tag{20}$$

Integrating the preceding differential equation produces

$$\frac{1}{2}\left(\frac{d\Theta}{ds}\right)^2 = \frac{P}{EI}\cos\Theta + C \tag{21}$$

which is in terms of deflection angle θ and not vertical deflection *y*. Differentiating and integrating Equation 18 does not yield the initial result because the coordinates are transformed from rectangular into angular deflection by Equation 20.

A schematic showing the location of x_o and l_o with respect to the link, which will be used in subsequent steps, can be seen in Figure 7.3. Note that the angle Θ_l is the maximum deflection angle with the horizontal and is located at the pinned end of the structure.

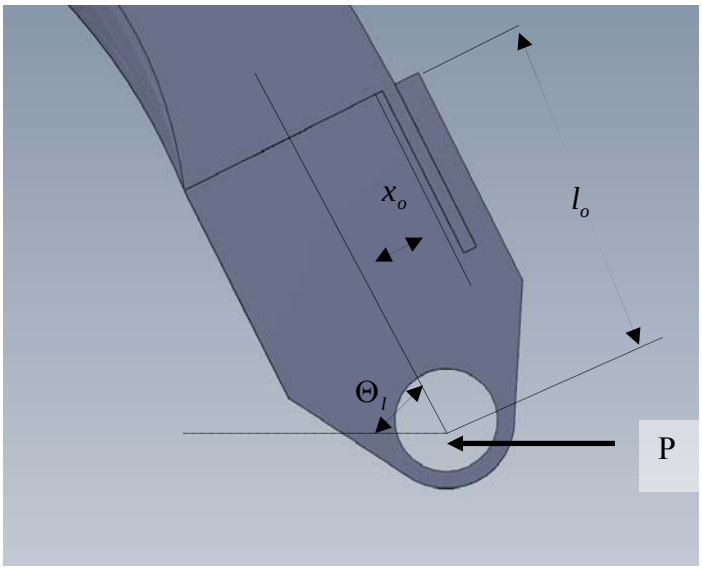

Figure 7.3. Coordinates for bending moment due to eccentric clamp on Smart Link

The moment imposed on the structure is caused by two phenomenons: the direct force on the tip of the beam (shown in Figure 7.3) and the bending moment caused by the offset of aluminum clamp. Note that the bending moment due to the directly applied force is zero when

the structure is fully straightened. The offset due to x_o and l_o on the clamp will result in a moment in *all* configurations, even when the beam is straightened. This offset moment is constant along the beam for a given deflection. If the offset within the clamp was not present, the structure would experience buckling when straightened and loaded. A free body diagram of both moments is shown in Figure 7.4.

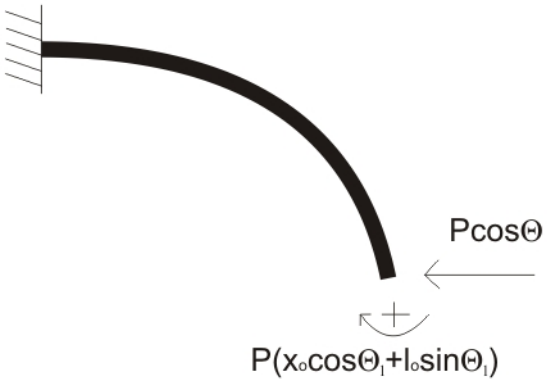

Figure 7.4. Free body diagram of constant moment due to clamp and moment varying along length

Equation 21 can be expanded with the following constraints: the radius of curvature equal R_o when P=0 and the moment equal $x_o \cos\Theta_l + l_0 \sin\Theta_l$ along the entire length of the beam when $\Theta = \Theta_l$. This result is shown in Equation 22.

$$\frac{d\Theta}{ds} = \sqrt{\frac{1}{R_o} + \frac{2P}{EI}\left(\cos\Theta - \cos\Theta_l + x_o \cos\Theta_l + l_0 \sin\Theta_l\right)} \tag{22}$$

or

$$ds = \frac{d\Theta}{\sqrt{\frac{1}{R_o^2} + \frac{2P}{EI}\left(\cos\Theta - \cos\Theta_l + x_o \cos\Theta_l + l_0 \sin\Theta_l\right)}} \tag{23}$$

where x_o = 0.275" and l_o=0.75".

The x-position at the tip of the beam can be written as a function deflection angle as shown in Equation 24. This is done by substituting Equation 23 in for *ds*.

$$x(l) = \int_0^l \cos\Theta ds = \int_0^{\theta_l} \frac{\cos\Theta d\Theta}{\sqrt{\frac{1}{R_o^2} - \frac{2P}{EI}\left(\cos\Theta - \cos\Theta_l + x_o \cos\Theta_l + l_0 \sin\Theta_l\right)}} \tag{24}$$

Assuming the modeled beam to be inextensible, the total length of the beam can be expressed as l_o, the initial and constant length, in Equation 25.

$$l = l_o = \int_o^l ds = \int_0^{\theta_l} \frac{d\Theta}{\sqrt{\frac{1}{R_o^2} - \frac{2P}{EI}\left(\cos\Theta - \cos\Theta_l + x_o \cos\Theta_l + l_0 \sin\Theta_l\right)}} \tag{25}$$

and every value of P can be calculated for each corresponding value of Θ_l since *l* is assumed to be constant.

Since the Smart Link is a composite structure with two distinct layers in the cross section, the second moment of area must be adjusted accordingly. The cross section can be converted to a homogeneous entity so that the entire cross section is made up of either nitinol or SMP. This process is done by calculating the ratio of Young's moduli between the two materials and then adjusting the width dimension of the according material. In this case the homogeneous material was chosen to be the thermally activated SMP. The cross section change due to moduli ratio is demonstrated in Figure 7.5.

Figure 7.5. Conversion of cross section to entirely SMP based on modulii ratio α

The moduli values of the SMP (E_p), nitinol (E_n), and moduli ratio α are shown in Equations 26, 27, and 28.

$$E_p = 29\ psi \tag{26}$$

$$E_n = 5*10^6\ psi \tag{27}$$

$$\alpha = \frac{E_n}{E_p} = 1.74*10^5 \tag{28}$$

The modulus value of the nitinol was assumed to be in the fully martensitic state and was taken from Johnson Matthey Inc. (2008). The polymer modulus value is that of the thermally activated state and was taken from Gross (2008).

In order to solve for input and deflection of the model, a numeric computation was completed. The final formulation contains two unknowns, P and Θ_l, so neither the input nor output could be solved for algebraically in one step. The computation was completed in the following manner: a value of P was chosen starting with 0, values of Θ_l starting with 0 were input with the same starting value of P, Θ_l was increased by a small increment until the solution converged (until Equation 25 held true with a convergence criterion of 0.00001), this value was recorded so that the starting value of P has a corresponding value of Θ_l, P was then increased by a small increment and the process was repeated so that all applicable values of load would have a

corresponding value of deflection. The Matlab script accompanying this numerical solution can be found in Appendix A.

The output of the theoretical model is plotted along with the measured data from the finalized Smart Link design in Figure 7.6.

The measured value was tested in the setup shown in Figure 3.14 in Chapter 3. The link, at an interior angle of 130 degrees, was placed into the pin assemblies in the clamp and the environmental chamber was set to 100 degrees Celsius and the polymer was allowed to transition fully. At this point, the nitinol created an expanding force due to the very soft polymer region. This force value (0.20 lbf.) was added to all subsequent force measurements since the load frame designates the first measurement as 0 lbf. In other words, the measured 0.20 lbf. was the preload within the hardened link.

The link was then compressed until an interior angle of 27 degrees was reached. Linear distance between the two pins was recorded as a function of load, and later converted to angular tip deflection for comparison with the theoretical model.

When comparing theory to the measurement, it can be inferred that the nitinol does in fact transition in majority to martensite since the difference between the theoretical and measured deflection decreases with increasing load. If the behavior before complete deformation was of design interest, then a more thorough model including phase transformation would need to be considered. Also, it can be noted that the measured data does not begin at a load of 0 because the measurement was initiated at an interior angle of 130 degrees with a residual load experienced by the link.

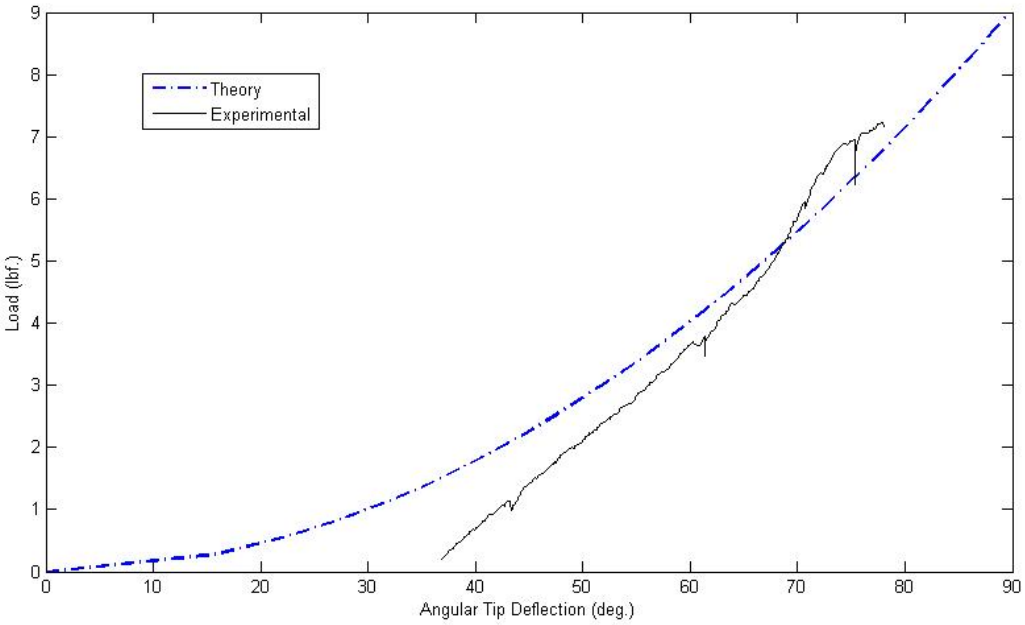

Figure 7.6. Plot of theoretical displacement and measured displacement vs applied load

When observing the behavior of the measured deflection values, one can notice some irregularities. First, the measured data starts at a load greater than 0 and this may be a point of confusion. For the test, the link was placed in the clamps at an interior angle of 130 degrees and thermally activated. After activation, an expansive force was applied to the load cell due to the stored energy within the nitinol. The load cell uses this initial force as a zero point, making the measurement inaccurate since there is a load exerted by the slightly compressed nitinol. In order to overcome this deficiency, the link was placed in the load frame while deactivated. The load cell was then set to measure instantaneous force and the environmental chamber was heated. As the SMP volume transitioned the internal expansive force of the nitinol was measured at 0.2 lbf. and added to the previously measured values for compensation.

One can also notice slight dips in the data at approximately 43, 60, and 73 degrees of deflection. These dips were captured because the frame was paused during the test to reset the

link. This resetting was done because the tie rods that connect the clamps to the frame were fairly long and narrow, allowing the pins to translate side to side and not remain in a straight vertical line. As the rods deflect more and more, the force measurement becomes distorted since the angle of the applied load changes. Because of this the test was paused and the link was slightly rotated to keep the pins in proper placing. The dip captured in the data was the instantaneous force captured by the load cell during rotation and should be ignored for comparison purposes.

The model and experimental are compared using the required force at the final deflection. It is important to note that both the theoretical and measured deflection are displayed as angular tip displacement (Θ_l). The schematic showing this value is displayed in Figure 7.1. The model is intended for use when analyzing final deflection since this value is important when trying to minimize necessary load for link closing. Therefore, deviation between theory and experiment before the final deflection are not considered to be a major consequence. The theoretical model predicted a necessary load of 6.540 lbf and the measured value was 6.925 lbf, creating a 5.9% error between the two at the final deflection with the theory slightly undershooting the measured values. These values easily fall within the design specification of 100 lbf.

This link design was also tested in the load frame to measure adherence to the 2 degree deflection tolerance in both the extended and collapsed state. The extended locked link deformed by an interior angle change of 1.4 degrees and the collapsed locked case experience an interior angle change of 0.44 degrees with 7 lbf. applied (the force required to collapse an activated link). While both results show passing values for the tolerance test, the relative magnitude of both contradict what should happen in theory. The extended case should deflect less since it is closer to being straight and possesses a smaller moment arm than in the collapsed

case. One cause for this discrepancy could be the out of plane rotation of the clamps explained earlier. Another reason could be that the SMP becomes denser after compression and is actually stiffer than when the link is fully extended. This phenomenon did occur when testing the extended case to a greater degree than with the collapsed link, so making a direct comparison between the two values may be futile since the loading conditions in both instances are not exactly the same.

8.0 WIND TUNNEL TESTING

After the design and fabrication was complete, the Smart Link was incorporated into the UAV designed and built by NextGen Aeronautics. This complete setup was tested at the Kirsten Wind Tunnel located on the University of Washington campus. Testing was done to quantify aerodynamic properties while the wings were in different stages of morphing and to confirm that the Smart Link was capable of multiple morphing cycles. Testing the overall performance of the link such as activation time was also a motivating factor for the wind tunnel test. The main characteristics considered for the test were ability of the link to fully deform within the wing structure, time for one complete cycle (time for link to fully heat and transition and then cool down), and the total number of cycles that one link could withstand before failure. Two pairs of links were installed for testing: a pair closest to the fuselage with one link on either side numbered 0 and 1 (pair A), and one pair in the next fan rib bays with one link on either side numbered 2 and 3 (pair B). The positioning of the links within the morphing region of the wing can be seen in Figure 8.1.

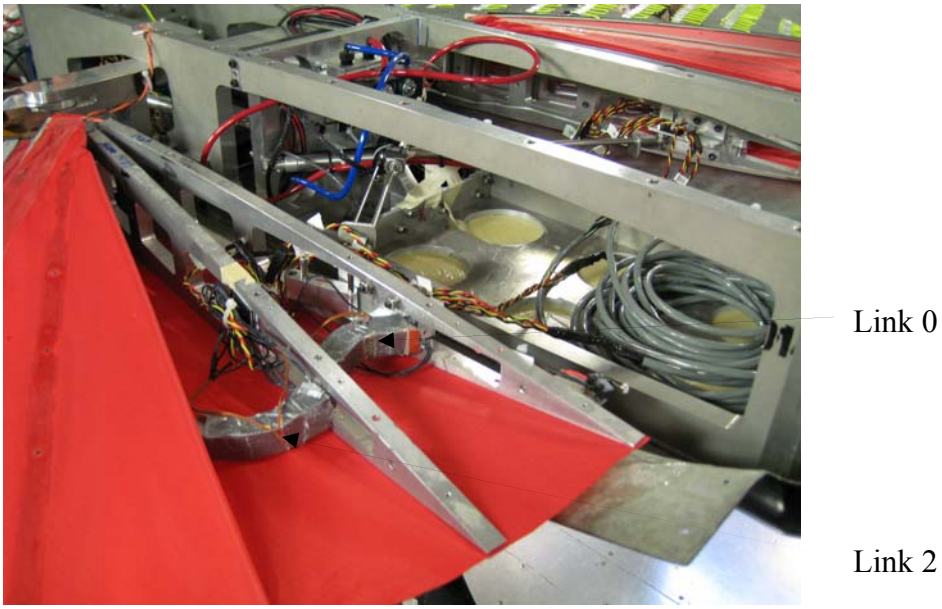

Figure 8.1. Labeled links (one of each pair) situated inside the morphing wing during test preparation

The silicone heating pads of a given link were wired in parallel with respect to the power supply. The power to all links was obtained from a single power supply that was located off-board the aircraft. This power was distributed by a set of relays (mounted in the aircraft fuselage) which were controlled by an off-board computer. During testing, all links were operated independently, but at most two were on at any given time (a pair of link in opposing fan rib bays).

In order to prepare for testing, four links were installed within the wings of the UAV. Two were placed in either wing in the positions closest to the fuselage as seen in Figure 8.1. The other open spots were occupied by a rigid link that could be locked and unlocked by a machine bolt. These rigid links remained locked during all testing.

During the first test the two links closest to the fuselage were activated and morphed. 11 V at 3 A were applied to all heating pads and both links were activated in 10 minutes. Temperature was monitored actively on a computer to know when the links were locked or unlocked. The activation point was considered to be 70 degrees Celsius for the first test since

environmental conditions inside the wind tunnel were unknown and a cycle without failure was considered more important than activation speed. At this point the links were successfully collapsed by an onboard pneumatic actuator, shown in Figure 8.2.

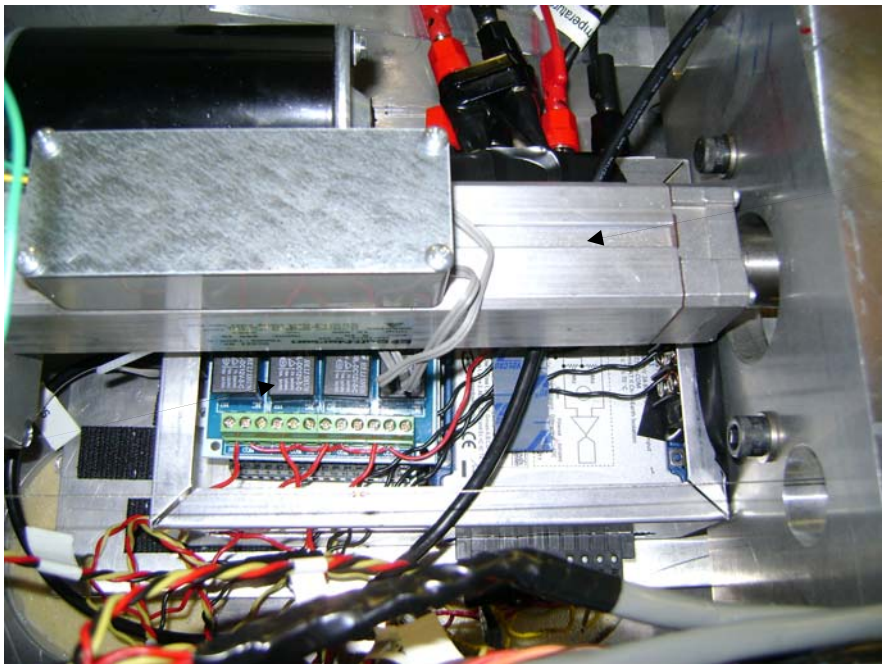

Figure 8.2. Pneumatic actuator and relay board layout in UAV fuselage

In order to complete the collapsing phase of the morphing cycle, the links had to cool to 30 degrees Celsius. Even though it is considerably lower than the activation temperature, this value was chosen to prevent failure due to still partially active regions within the polymer and assure that the pad interfaces were below activation temperature. The cooling process took 23 minutes for both links to harden sufficiently. The rib spacing was measured before and after the actuator force was removed from the links and there was no measurable change. This implies that the links were fully locked and there was not creep strain after the actuator force was removed.

The next step in the process required the collapsed links to be heated and pulled apart. A slightly higher amount of power, 12 V at 3.5 A, was sent to the pads on this part of the cycle. Activation time was clocked at 11 minutes for an activation temperature of 70 degrees. This time was slightly slower than the initial because the pad opposite of the nitinol side had less surface area in contact with the polymer due to compression during bending. In other words, part of the pad overlaid the aluminum clamp and did not contribute to heating the SMP. This phenomenon is shown in Figure 8.3.

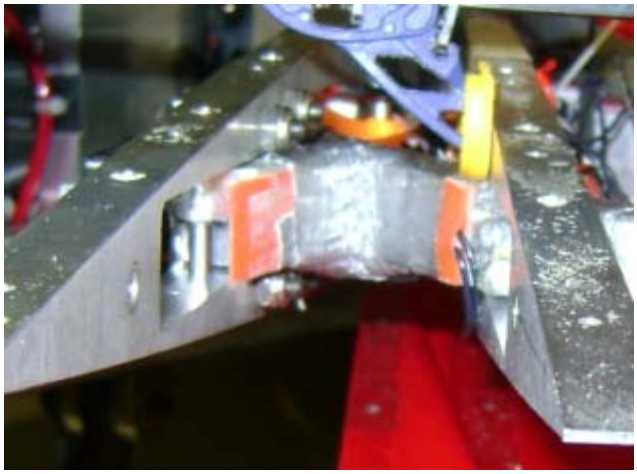

Figure 8.3. Collapsed link displaying heating pad overlay on clamps after compression

Actuator pressure was applied in the opposite direction to pull apart the ribs and was held until the links hardened. The cooling took 25 minutes and the actuator force was removed afterwards without any movement in the ribs. This complete process represents one successful morphing cycle of the UAV.

The next morphing attempt was halted mid-way due to heating pad failure. Failure occurred because the pad pulled away from the link and began to burn and smoke. This malfunction was not due to a flaw in the design, but rather the adhesive tape failing to securely hold the pad to the link interface. The burned link was swapped out with an unused assembly and testing proceeded.

The same links (pair A) next began another morphing cycle. Heating was done similarly to the previous test and the thermal response is shown in Table 3.

Table 3. Test 2 thermal response of links after pads are turned on

Time (s)	Link 0 Temp (°C)	Link 1 Temp (°C)
80	33	31
240	47	42
340	60	53
380	70	61
485	73	69

The links were then compressed again (the wing was morphed) and the power was deactivated to allow the polymer to cool. Actuator pressure was maintained to prevent spring back. The cooling response is displayed in Table 4.

Table 4. Test 2 thermal response of links after pads were turned off

Time (s)	Link 0 Temp (°C)	Link 1 Temp (°C)
130	60	63
230	55	57
330	50	53
430	46	48
535	42	44
630	39	41
730	37	38
835	35	36
940	33	34
1030	31	33
1130	30	31
1205	29	30

After cooling, the pressure was released with no noticeable movement in the wing. Next, the second pair of links (pair B) was successfully morphed for one full cycle using the same process as the first two tests. Thermal data is shown in Tables 5 and 6 below. The links were powered at 12 V at 3.4 A. Link 3 reached activation temperature much earlier than link 2 and its power was toggled to prevent overheating.

Table 5. Test 3 thermal response of links after pads are activated

Time (s)	Link 2 Temp (°C)	Link 3 Temp (°C)
95	41	41
200	52	63
240		70
290	59	75
395	64	72
495	67	76
590	70	73

Table 6. Test 3 thermal response of links after pads are deactivated

Time (s)	Link 2 Temp (°C)	Link 3 Temp (°C)
160	62	68
265	57	61
360	57	56
460	53	51
550	50	48
655	46	44
770	43	41
855	40	39
950	38	37
1055	36	35
1403	32	32
2040	30	30

Next, the links were heated again and expanded using the same process as the first test. However, during heat one of the links failed to register a temperature reading above 44 degrees Celsius. After the other reached activation, the actuator was used and the link with the low temperature morphed properly. It was discovered that the temperature increased on the faulty readout after the morph, making it possible that the thermocouple disengaged and was reengaged during the morph. The links were cycled thermally again and the wings successfully extended.

Pairs A and B were then both morphed again for one full successful cycle each. Pair B was morphed without allowing the links to cool; the links were compressed and immediately extended and then compressed and cooled. While extended, pair B was thermally activated to 67 degrees Celsius in a time of 3:23 while the pads were powered with 13 V at 3.6 A . This was the

fastest that any of the links was activated and was able to successfully bend without failure. Pair A was morphed 3 complete cycles and pair B was morphed one complete cycle and a second cycle that did not include link hardening after compression (the links were compressed and then extended without allowing time to cool in between). Temperature data for this test and all other morphing tests can be found in Appendix C.

9.0 CONCLUSIONS AND FUTURE WORK

This research investigated the use of shape memory polymer as a viable candidate for a morphing structure. The use of the polymer in the Smart Link was a success in that it allowed NextGen's morphing UAV to successfully morph several cycles during wind tunnel testing. The SMP was not considered a perfect success because it took between 3 and 4 minutes to activate and even more to cool down. This transient response may be a limiting factor when considering practical implementation of the Smart Link in a morphing aircraft application.

The activation time of the polymer in the morphing setup may possibly be made more efficient with greater initial analysis of the aircraft. For instance, since force requirements were not specified, it may have been possible to successfully implement a link with a much thinner polymer region that could transition more quickly.

Also, a composite cross section, similar to the one presented by McKnight et al. in the literature review, could also decrease activation time. This composite structure, shown in Figure 9.1, would allow faster transition since multiple layers of very thin nitinol replace one larger section and permit faster heat transfer along the entire cross section. Note that the thickness of the nitinol strips would need to be considerably thinner than the once piece used in the actual design (approaching the thickness of foil) in order to permit deflection under a reasonable load.

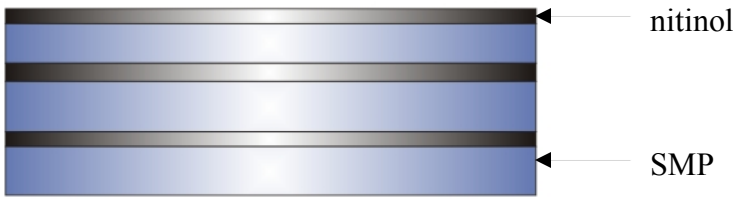

Figure 9.1. Composite cross section of thin nitinol layers and SMP

Lastly, it is recommended that another smart material be considered for the morphing wing setup. There is a physical limit with how fast the shape memory polymer can transition due to its maximum working temperature, so thermal design can only improve the transient response by a moderate amount. Ideally, a material that is not activated by thermal energy would be considered. Depending on the performance of such a material, the link could possibly be activated and deactivated within seconds instead of minutes.

APPENDIX A

MATLAB SCRIPT FOR DEFLECTION MODEL

```
clear all
format long

%material properties
Es=5e6;
Ep=29;
alpha=Es/Ep;

%dimensions
h1=.020;
h2=(.55);
y1=h2+h1/2;
y2=h2/2;
b=0.75;

%center of mass calculation
Atot=alpha*b*h1+b*h2;


ybar=(1/Atot)*((y1)*(alpha*b*h1)+(y2)*(b*h2));

c=0.5-ybar;

%inertial calculation
I1=(alpha*b*h1^3)/12;
I2=(b*h2^3)/12;

I=I1+((h2-ybar)+h1/2)^2*(alpha*b*h1)+I2+(ybar-h2/2)^2*(b*h2);


%initial radius of curvature
ro=10000000000000000000000000000000000;
%effective beam length (length of SMP/nitinol section only)
l=1.45;
```

```
%offset dimensions of clamp
lo=.75;
xo=.275;



%begin convergence calculation of Gonzalez/Llorca model
P=0;
thetal=0;
int(:,1)=0;
n=2;
m=1;
o=1;
delta=1;
count=1200;
loadcount=8;


while P<=loadcount



while real(delta)>=0.00001


    while n<=count+1
    interval=(thetal/count);
    int(:,n)=int(:,n-1)+interval;
    n=n+1;
    end



    while m<=count+1
        f(:,m)=1/(sqrt(1/(ro^2)+((2*P)/(Ep*I))*(cos(int(:,m))-
cos(int(:,count+1))+xo*cos(thetal)+lo*sin(thetal))));
        m=m+1;
    end

    m=1;
    while m<=count
        a(:,m)=((f(:,m)+f(:,m+1))/2)*interval;
        m=m+1;
    end

    integral=sum(a);


    delta=l-integral;

    thetal=thetal+.001;
    n=2;
```

```
end

output(:,o)=(thetal-.001)*(180/pi);
o=o+1;
P=P+.25;
thetal=0;
int(:,1)=0;
n=2;
m=1;
delta=1;
count=1500;

end

P=linspace(0,loadcount+1,length(output));
data=xlsread('finallink.xls');

%convert pin-to-pin deflection to angular tip displacement used in model
x=acos((3.6-data(:,2))/4.5)*(180/pi);

f=data(:,1)+.2;



plot(output,P,'-.');
hold on;
plot(x,f,'black');
hold off;
ylabel('Load (lbf.)');
xlabel('Angular Tip Deflection (deg.)');
```

APPENDIX B

MATLAB SCRIPT FOR TRANSIENT THERMAL ANALYSIS MODEL

```
clear all
format long

%initial temp of slab (25 deg. C) compensated for boundary conditions;
To=-110;

c=(4*To)/pi;

%width of slab converted from 0.55" to meters
l=.01651;

n=1;

%thermal diffusivity
alpha=102.7e-9;

x=0;
delta=l/50;
m=1;
count=1;
increment=linspace(1,12,12);
countt=1;


%calculate heat equation output for given initial conditions
for x=0:delta:l

for t=0:32:1600

while n<=1000

T(n)= (1/n)*exp(-alpha*((n*pi)/l)^2*t)*sin(((n*pi)/l)*x);

n=n+2;

end
```

```
Ttot=c*sum(T);
Tt(count,countt)=Ttot+135;


n=1;
count=count+1;
end

count=1;


countt=countt+1;

end


%plot 3d contour of response and response mid-way within slab
figure(1)
t=linspace(0,50,51);
plot(t,Tt(:,26)+135);

x=(0:delta:l);
t=0:32:1600;
figure(2)
surf(x/l,t,Tt)
```

APPENDIX C

THERMAL DATA FOR MORPHING TESTS

Table 7. Test 3 thermal response of links after pads were turned on during compression

Time (s)	Link 2 Temp (°C)	Link 3 Temp (°C)
100	46	35
200	64	49
300	60	53
400	58	45
500	63	44
600	66	44
700	68	44

Table 8. Test 3 thermal response of links after pads were turned off during compression

Time (s)	Link 2 Temp (°C)	Link 3 Temp (°C)
300	56	68
450	48	62
550	44	58
650	41	54
750	38	50
850	35	47
950	33	44
1050	32	41
1100	31	40

Table 9. Test 4 thermal response of links after pads were turned on during extension

Time (s)	Link 2 Temp (°C)	Link 3 Temp (°C)
100	37	34
200	48	42
300	59	52
400	69	61
500	69	67

Table 10. Test 4 thermal response of links after pads were turned off during extension

Time (s)	Link 2 Temp (°C)	Link 3 Temp (°C)
100	63	70
200	59	65
300	54	60
400	50	56
500	47	52
600	44	48
700	41	45
800	39	42
900	37	40

Table 11. Test 5 thermal response of links after pads were turned on during compression

Time (s)	Link 0 Temp (°C)	Link 1 Temp (°C)
100	37	32
200	51	44
300	65	54
400	70	66
440	70	67

Table 12. Test 5 thermal response of links after pads were turned off during compression

Time (s)	Link 0 Temp (°C)	Link 1 Temp (°C)
90	73	67
190	67	63
290	61	56
390	56	50
490	51	45
590	47	41
690	43	37
790	40	35

Table 13. Test 6 thermal response of links after pads were turned on during compression

Time (s)	Link 2 Temp (°C)	Link 3 Temp (°C)
0	37	37
100	50	53
200	66	72
212	67	72

Table 14. Test 6 thermal response of links after pads were turned off during extension

Time (s)	Link 2 Temp (°C)	Link 3 Temp (°C)
0	55	58
100	48	50
200	43	45
300	40	42
350	39	40

Table 15. Test 6 thermal response of links after pads were turned on during extension

Time (s)	Link 0 Temp (°C)	Link 1 Temp (°C)
0	40	39
100	48	42
200	61	49
300	71	59
400	71	66

BIBLIOGRAPHY

A modified F/A-18A undergoes wing torsion or twist testing in the Flight Dynamics Lab at NASA-Dryden. September 2002. American Institute of Aeronautics and Astronautics (AIAA). 9 November 2008 <http://www.aiaa.org/Aerospace/Article.cfm?issuetocid=256&ArchiveIssueID=30>

Air Force Link - Leonardo da Vinci. United States Air Force. 9 November 2008 < http://www.af.mil/history/leonardodavinci.asp>

CRG Technology - Morphing Systems. Cornerstone Research Group, Inc. 9 November 2008 < http://www.crgrp.com/morphingsystems.shtml>

Flanagan, John S. "Development and Flight Testing of a Morphing Aircraft, the NextGen MFX-1." 48th AIAA Structures, Structural Dynamics, and Materials Conference 2007: 73-75.

González, C. LLorca, J. "Stiffness of a curved beam subjected to axial load and large displacements." International Journal of Solids and Structures. 42 (2005): 1537-1545.

Gross, Korey. "Mechanical Characterization of Shape Memory Polymers to Assess Candidacy as Morphing Aircraft Skin." Thesis. University of Pittsburgh, 2008.

Grumman Aerospace Corporation. Aerial photo of the F-14. 9 November 2008 < http://history.nasa.gov/SP-4406/4406-053.jpg>

Henry, Chris. McKnight Geoff. "Variable Stiffness Materials for Reconfigurable Surface Applications." Smart Structures and Materials 2005: Active Materials: Behavior and Mechanics 2005: 119-129.

Jha, Akhilesh K. Kudva, Jayanth N. "Morphing Aircraft Concepts, Classifications, and Challenges." Smart Structures and Materials 2004: Industrial and Commercial Applications of Smart Structures and Technologies. 2004: 213-224.

Lendlein, Andreas. Langer, Robert. "Biodegradable, Elastic Shape-Memory Polymers for Potential Biomedical Applications." Science. 296 (2002): 1673-1676.

Leo, Donald J. Engineering Analysis of Smart Material Systems. Hoboken, NJ: John Wiley & Sons Inc., 2007.

Liu, C. Mather, P. T. Qin, H. "Review of progress in shape-memory polymers." Journal of Materials Chemistry 19 March 2007: 1543-1558.

Miyazaki, S. Sandström, R. Wei, Z. G. "Shape-memory materials and hybrid composites for smart systems." Journal of Materials Science 22 April 1998: 3743-3762.

NASA - NASA Dryden Fact Sheet - Active Aeroelastic Wing. 8 May 2008. NASA. 9 November 2008 < http://www.nasa.gov/centers/dryden/news/FactSheets/FS-061-DFRC.html>

Next Gen Aeronautics / Success Stories - MFX-1 Flight Test. 2007 NextGen Aeronautics Inc. 9 November 2008 <http://www.nextgenaero.com/success_mfx1.html>

Next Gen Aeronautics / Success Stories - MFX-2 Flight Test. 2007 NextGen Aeronautics Inc. 9 November 2008 <http://www.nextgenaero.com/success_mfx2.html>

Nitinol Technical Properties. 2008. Johnson Matthey. 3 December 2008 <http://jmmedical.com/resources/221/Nitinol-Technical-Properties.html>.

Özişik, Necati. Heat Transfer: A Basic Approach. North America: McGraw-Hill Inc., 1985.

Rauscher, Scott G. "Testing and Analysis of Shape-memory Polymers for Morphing Aircraft Skin Application." Master of Science Thesis. University of Pittsburgh, 2008.

Smart suture is first application of novel MIT polymer. 22 April 2002. Massachusetts Institute of Technology. 2 December 2008 < http://web.mit.edu/newsoffice/2002/langer-suture.html>.

Transition range graph. CRG Industries, LLC., 10 November 2008 <http://crgindustries.com/images/tg-range.gif>.

Veriflex. 2005. CRG Industries, LLC. 10 November 2008 < http://www.crgindustries.com/veriflex.htm>.